Titre: Title:	Inverse heat conduction problem in a cavity
Auteur: Author:	Jiang Chen
Date:	1998
Type:	Mémoire ou thèse / Dissertation or Thesis
Référence: Citation:	Chen, J. (1998). Inverse heat conduction problem in a cavity [Mémoire de maîtrise, École Polytechnique de Montréal]. PolyPublie. https://publications.polymtl.ca/6864/

UNIVERSITÉ DE MONTRÉAL

INVERSE HEAT CONDUCTION PROBLEM IN A CAVITY

JIANG CHEN
DÉPARTEMENT DE GÉNIE MÉCANIQUE
ÉCOLE POLYTECHNIQUE DE MONTRÉAL

MÉMOIRE PRÉSENTÉ EN VUE DE L'OBTENTION
DU DIPLÔME DE MAÎTRISE ÈS SCIENCES APPLIQUÉES
(GÉNIE MÉCANIQUE)

JANVIER 1998

UNIVERSITÉ DE MONTRÉAL

ÉCOLE POLYTECHNIQUE DE MONTRÉAL

Ce mémoire intitulé:

INVERSE HEAT CONDUCTION PROBLEM IN A CAVITY

Présenté par: CHEN Jiang

en vue de l'obtention du diplôme de: Maîtrise ès sciences appliquées

a été dûment accepté par le jury d'examen constitué de:

M. MICHEL PRUD'HOMME, Ph.D., Président

M. THE HUNG NGUYEN, Ph.D., membre et directeur de recherche

M. LUC ROBILLARD, D.Sc.A., membre et codirecteur de recherche

M. RENÉ KAHAWITA, Ph.D., membre

To my parents

ACKNOWLEDGEMENTS

First of all, I would like to express my greatest appreciation to professor T. Hung Nguyen, my master program supervisor, for his encouragement and guidance in all phases of my graduate studies in the Department of Mechanical Engineering, Ecole Polytechnique, University of Montreal in the past two years. I consider it a great pleasure to study and work under his supervision and consultant. I believe that his profound interpretation to the phenomena of nature and ingenuity in doing scientific research will considerably influence my entire life of career.

I also would thank my co-director, Professor Luc Robillard and other professors of our group. I will never forget the help from the fellow graduate students in the department for their help in various form. Especially I should thank Ji Ma, Ning Zhang, Wei Bian, Min Zhao and Mohamed Mamou of our group and Stéphane Hallé, Idriss Amara, Valérie Patreau and Frédéric Genest who are from my office. Furthermore I would mention the continuous technical support I received from Alain Robidoux and Daniel Laporte, system administrators of the department.

Finally, I should thank the Ministère de l'Education du Québec for the waiver of the foreign tuition fees of my first year and the Ecole Polytechnique for its dynamic and scientific atmosphere as well as the financial support during my study.

RÉSUMÉ

L'objectif de ce mémoire est de résoudre le problème inverse de conduction bi-dimensionnelle par deux méthodes différentes dont l'une est une méthode directe, soit la méthode de marche, et l'autre est une méthode itérative, soit la méthode d'optimisation par gradient conjugué. Dans chaque cas, les effets des erreurs numériques et expérimentales seront analysés à chaque étape principale de l'algorithme de solution. Les mécanismes de régularisation par mollification et par itération seront ensuite étudiés en détails.

Nous démontrerons d'abord que la méthode de marche est très instable à la fois par rapport aux erreurs dans les données et aux erreurs des calculs numériques effectués au cours de la marche vers la frontière inconnue. La croissance de ces instabilités dépend fortement du maillage de calcul et des positions des senseurs relatives à la frontière inconnue. Pour contrôler ces instabilités, nous avons recouru à la technique de mollification, en utilisant trois différents types de filtre, soit un filtre gaussien, un filtre carré et un filtre Dirichlet. Une des conséquences de cette technique est que la solution peut être fortement déformée par le processus de mollification. Par conséquent, la précision de cette méthode est très difficile à déterminer.

Nous traiterons ensuite le problème inverse de conduction sous la forme d'un problème d'optimisation qui consiste à trouver un flux de chaleur qui engendra des températures aussi proches que possible des températures mesurées. Il s'agira alors d'un problème de minimisation dans un espace fonctionnel de dimension in-

finie que nous pouvons résoudre par une méthode itérative par gradient conjugué. Nous démontrerons que cette méthode est très robuste et peut être appliquée à une grande variété de problème. Son mécanisme de régularisation réside dans le processus d'itération tel que la structure globale de la solution est révélée dès les premières itérations, tandis que sa structure fine et les instabilités dues aux erreurs de mesures se manifestent seulement après un assez grand nombre d'itérations. Un critère d'arrêt basé sur un nombre d'itération optimal permettra ainsi d'obtenir une solution à la fois stable et précise. Nous montrerons finalement que cette méthode s'applique aussi bien aux problèmes permanents qu'aux problèmes transitoires.

En conclusion, nous recommandons la méthode d'optimisation par gradient conjugué à cause de sa robustesse et sa généralité, tout en pensant à la méthode de marche pour une première estimation rapide et une implantation facile.

ABSTRACT

The objective of this thesis is to solve the ill-posed 2D IHCP by two different methods, namely the space marching method and the optimization method by conjugate gradient.

In each case, the effects of numerical errors and measurements errors on the inverse solutions are analyzed at each step of the algorithm. The regularization effects of filtering by mollification and iteration are next studied in details.

We first show that the space marching method is very unstable not only against random errors in the given data, but also against numerical errors which are generated by computational truncations during the marching process. The development of these instabilities depends strongly on the relative grid size as well as on the cavity size. In fact, one should expect that the marching method is unconditionally unstable, as it directly solves the 2D IHCP in the original form of an initial-value problem with Cauchy data. In order to suppress these instabilities, we should suppress their origin, i.e., both the experimental and computational errors! This can be done by applying a low-pass filter at every step of the marching process. Although filtering technique is efficient to suppress high-frequency noises, it may also distort the "true" temperature field. The distorsion of the solution, as well as the suppression of undesired high-frequency noises, depend sensibly on the type of filter and the number of times it is applied. Among the three types of filters considered, namely the Square filter, the Dirichlet filter and the Gaussian filter, it was found that the

last one may be a good choice for a good number of unknown functions.

We next consider the 2D IHCP from an optimization point of view. The problem then consists of finding iteratively a boundary heat flux that would induce a temperature as close as possible to the one measured by sensors located within the given cavity. This amounts to solving a minimization problem in an infinite-dimensional function space by the conjugate gradient technique. It was found that numerical truncation errors also strongly affect the final results, but in a very different way from the space-marching method. More specificly, it was found that numerical errors make the step size in the search direction vanishingly small compared to the analytical value as the frequency of the given data is increased and/or the sensors are moved further away from the unknown boundary. Therefore, convergence towards the expected value can not be reached. This may be considered as a beneficial regularization effect in the sense that if the high-frequency components of the data one due to measurement errors, they will not affect the solutions! However, if these high-frequency components are parts of the real data, then the corresponding boundary heat flux that causes them can not be recovered! By looking for a "right" position to place the sensors, we may therefore arrive at solution with acceptable accuracy and stability.

Furthermore, we analyzed the convergence mechanism of the iterative conjugate gradient algorithm by considering given data with multifrequency components. It was found that as the iteration progresses, the first iteration recovers mainly the lowest frequency component of the unknown heat flux, the second iteration yields the next higher frequency component, and so on. Very high frequency components will be recovered only at high iteration number. This is the very desirable regularization effect intrinsically embedded in the iterative algorithm of solution by conjugate gradient. In other words, a choice can be made of an optimum iteration number to arrive at a regularized solution with acceptable accuracy and stability.

Finally, it was verified that the results obtained for the steady state 2D IHCP also apply to the time-dependent 2D IHCP: Using the conjugate gradient technique in conjunction with a low-pass Gaussian filter applied to the noisy data, a very smooth and accurate solution was obtained by an appropriate combination of sensors' positions and iteration number.

As a conclusion, we may make the following recommendation for solving the ill-posed 2D IHCP:

1. For diagnostic and control purposes where a rough estimate of boundary heat flux is sufficient and a fast prediction is necessary, space marching technique may be used with an appropriate choice of a low-pass filter.

2. For an accurate prediction of boundary heat flux or for more general inverse heat transfer problems, the conjugate gradient method should be used in conjunction with a low-pass filter applied to the given data.

CONDENSÉ EN FRANÇAIS

Durant les dernières années, les problèmes inverses en transfert de chaleur ont reçu un intérêt croissant. Les recherches dans ce domaine ont été dictées par le développement des hautes technologies dans lesquelles l'analyse et le contrôle de l'état thermique d'un système ou d'un procédé conduisent généralement, sous une forme ou une autre, à un problème inverse, ce dernier s'inscrivant à l'encontre du principe de causalité. Mathématiquement parlant, un problème inverse est un problème mal posé, au sens de Hadamard, c'est-à-dire que la solution n'existe pas, ou n'est pas unique, ou encore elle n'est pas une fonction continue des données.

Un des premiers exemples de problème inverse est la détermination du flux de chaleur à la surface des vaisseaux spatiaux lors de la rentrée dans l'atmosphère terrestre. La connaissance de ce flux (qui est due à l'échauffement par la friction de l'air) est indispensable pour le design de la gaine de protection de ces engins. Pour déterminer ce flux, on doit se baser sur des mesures de température prises en dessous de cette surface, Autrement dit, on doit déterminer la condition thermique à la surface d'un corps solide à partir des températures à l'intérieur de ce corps.

La difficulté fondamentale des problèmes inverses est due au fait que leurs solutions sont généralement instables, c'est-à-dire qu'elles peuvent varier largement même si les données n'encourent que des changements infinitésimaux. Ainsi, le premier objectif des travaux sur les problèmes inverses consiste à trouver des techniques pour stabiliser ou , dans un langage plus spécifique, régulariser les solutions,

lorsqu'elles existent.

Différentes méthodes de solutions ont été développées durant les dernières décennies. La plupart de ces méthodes ont été appliquées au problème de conduction inverse à une dimension, lequel représente en effet un problème canonique pour le développement de différentes techniques de solutions et de régularisation. Une bibliographie assez complète des travaux publiés en Occident est donnée dans le livre de Beck et al, tandis qu'une bibliographie des travaux russes est présentée dans le livre de Alifanov.

En pratique, on rencontre plus fréquemment des problèmes bi-dimensionnels, voire tri-dimensionnels. D'un autre coté, les méthodes de solutions développées pour les problèmes mono-dimensionnels ne s'adaptent pas toujours très bien aux problèmes à plusieurs dimensions.

Ce mémoire est consacré au problème inverse de conduction bi-dimensionel qui consiste essentiellement à déterminer le flux de chaleur sur un coté d'une plaque rectangulaire, en se basant sur les conditions thermiques données sur les trois autres cotés, et sur les mesures de températures prises sur le coté opposé (ou à l'intérieure) de la plaque.

L'objectif principal de ce travail est de résoudre le problème inverse de conduction par deux méthodes différentes, dont l'une est directe, soit la méthode de marche et l'autre itérative, soit la méthode d'optimisation par gradient conjugué. Chaque méthod e sera analysée en détail dans le but de révéler les symptomes et/ou difficultés inhérentes à la nature du problème inverse (problème mal posé) La question principale à répondre concerne évidemment la stabilité des solutions obtenues par chaque méthode. Aussi, nous analyserons en détails l'influence des erreurs de mesures de température sur la stabilité des solutions obtenues par chaque méthode.

Ce mémoire comporte de six chapitres.

Dans le premier chapitre, nous présenterons d'abord une introduction générale aux problèmes inverses et à leurs applications en transfert de chaleur, suivie d'une bibliographie du problème que nous allons traiter, soit le problème de conduction inverse aux conditions frontières inconnues. Nous définissons ensuite l'objectif de notre travail, à savoir la solution du problème inverse de conduction bi-dimensionnelle à frontière inconnue par la méthode de marche et la méthode d'optimisation par gradient conjugué. Plus spécifiquement, notre travail consiste en une étude des techniques de régularisations utilisées dans chaque méthode, soit la technique de mollification incorporée dans la méthode de marche et l'algorithme d'itération par gradient conjugué dans la méthode d'optimisation, la précision et la stabilité des deux approches étant finalement comparées.

Le deuxième chapitre décrit le problème que nous allons traiter aux chapitres suivants, soit le problème inverse de conduction dans une plaque rectangulaire dont le flux de chaleur sur un coté est inconnu, et doit etre déterminé à partir des mesures de températures sur le coté opposé, ou à l'intérieur de la plaque. Nous décrirons ensuite les deux méthodes de solution pour résoudre ce problème, soit la méthode de marche et la méthode d'optimisation.

Dans le troisième chapitre nous traiterons le problème de conduction en régime permanent dans un rectangle dont les conditions thermiques sur les trois cotés (nord, sud, ouest) sont connues, mais dont le flux de chaleur sur le quatrième coté (coté est) est inconnu. Pour compenser cette absence de condition frontière, nous disposons de mesures de température sur la frontière ouest comme données supplémentaires. Dans notre étude numérique, ces températures sont simulées en résolvant le problème direct avec un flux de chaleur donné sur le coté est du rectangle. Ce flux représente ainsi la solution que nous devons retrouver en résolvant le problème inverse avec des températures simulées précédemment. Avec le flux de chaleur et la température sur le coté ouest comme données de départ, nous pouvons exécuter une marche

vers l'est avec un schéma de discrétisation de l'équation de conduction par volume de contrôle. Nous discuterons en détail l'influence du maillage et de la forme des données du problème sur la stabilité de la solution, et nous démontrerons, en particulier, la croissance exponentielle des erreurs numériques aussi bien que des erreurs dans les données (c.à.d. dans les mesures de températures). En fait, cette croissance exponentielle reflète simplement la nature mal-posée du problème qui est résolue ici comme un problème aux valeurs initiales de Cauchy. Pour contrôler la croissance de ces erreurs, nous utiliserons trois types de filtre, soit le filtre gaussien, le filtre carré et le filtre Dirichlet. L'application d'un filtre sur les données entraîne cependant un déformation de ces données, tout en éliminant des erreurs indésirables. Cette déformation entraîne à son tour une perte de précision de la solution que nous devons accepter comme un prix à payer pour sa stabilité. La perte de précision de la solution, de même que l'élimination des erreurs des mesures, dépendent du type de filtre utilisé et du nombre de fois qu'il est appliqué durant la marche vers la frontière inconnue. En général, le filtre gaussien est un bon choix pour un bon nombre de cas, et nous pouvons conclure que la méthode de marche, utilisée conjointement avec la technique de mollification, est une méthode rapide et facile à implanter, mais la précision de la solution est très difficile à contrôler, surtout dans les problèmes bidimensionnels.

Le chapitre 4 traite le problème inverse de conduction sous la forme d'un problème d'optimisation. Il faudra alors trouver, dans un espace de fonctions à dimension infinie, un flux de chaleur qui produirait des températures aussi proches que possible des températures données. Le problème consiste à minimiser une fonctionnelle par une méthode itérative. Dans cette étude, nous avons choisi la méthode d'optimisation par gradient conjugué. Nous montrerons que la convergence de cette méthode dépend des erreurs de calculs numériques et de la distance des senseurs par rapport à la frontière inconnue, comme dans la méthode de marche. Elle dépend

également de la structure des données. En général, les premières itérations recouvrent d'abord la structure globale (à grande échelle spatiale) du flux inconnu. La structure fine (à petite échelle spatiale) de la solution, de même que les instabilités dues aux erreurs aléatoires des mesures, se révéleront seulement après un assez grand nombre d'itérations. Ce processus de convergence itérative par gradient conjugué représente ainsi un excellent mécanisme de régularisation de telle sorte qu'un choix optimum du nombre d'itération permettra d'obtenir une solution suffisamment stable et précise. Nous arriverons alors à la conclusion que la méthode d'optimisation par gradient conjugué est une méthode de solution très robuste qui peut être appliquée à une gamme de problèmes beaucoup plus large et variée que la méthode de marche.

Le chapitre 5 traite du problème de conduction bi-dimensionnelle avec dépendance temporelle en utilisant la méthode d'optimisation par gradient conjugué. Les résultats obtenus montrent que cette méthode s'applique aussi bien aux problèmes permanents qu'aux problèmes transitoires. En plus, sa stabilité peut être améliorée en l'utilisant conjointement avec la technique de mollification pour réduire les erreurs aléatoires dans les données.

A titre de conclusion présentée au dernier chapitre, nous ferons les recommandations suivantes :

1. Pour avoir une première estimation du flux de chaleur frontalier à partir des mesures de températures relativement précises par des senseurs placés assez près de la frontière inconnue, la méthode de marche peut être choisie à cause de son implantation facile et de son exécution rapide.

2. Pour avoir une estimation plus précise, et pour des problèmes inverses plus généraux, la méthode d'optimisation par gradient conjugué sera plus fiable et précise, surtout si elle est utilisée conjointement avec la technique de mollification.

TABLE OF CONTENTS

LIST OF TABLES

LIST OF FIGURES

LIST OF SYMBOLS

D	boundary
E	object fucntional of optimization
e	propagated error in marching method
G_0	heat flux boundary condition
F_0	temperature boundary condition
$H(r)$	unkown boundary condition
H_0	height of studied region, m
h	convection coefficient, $W/(m^2 \cdot K)$
I	mesh size in x coordinate
J	mesh size in y coordinate
K_D	Dirichlet kernel
K_G	Gaussian kernel
K_S	Square kernel
k	thermal conductivity, $W/(m \cdot K)$
L_0	length of studied region, m
L	dimensionless length of studied region
p	optimization direction
q	unknown boundary heat flux
q_0	boundary heat flux at the measured boundary
r	dimensionless coordinate position vector

r'	coordinate position vector, m
$rand$	random number between -0.5 and 0.5
S	dimensionless internal heat source term
S'	internal heat source term, K/m^2
S_f	heat source term scale
T	dimensionless termperature
T'	temperature, K
$\Delta T'$	temperature scale
Tm	measured temperature
t	time, s
t'	dimensionless time
$\Delta t'$	time scale
x	dimensionless coordinate
x_o	sensors's location
Δx	length of control volume
y	dimensionless coordinate
Δy	height of control volume

Greek Symbols

α	thermal diffusivity, m^2/s
β	mesh aspect ratio
ϵ	optimization convergence criterion
ρ	conduction media density, kg/m^3
∇	gradient operator
$\nabla\cdot$	divergence operator
∇^2	Laplacian operator

Superscripts

$'$	refers to dimensional variables
$*$	refers to adjoint variables
$\tilde{}$	refers to temperature sensitivity
k	refers to optimization iteration step

Subscripts

est	refers to estimated value
i	refers to node series number in x coordinate
j	refers to node series number in y coordinate
m	refers to measured value or boundary
max	refers to maximum value

CHAPTER I

INTRODUCTION

Since the last two decades, inverse heat transfer problems have received an increasing interest in the theory and applications of heat transfer processes as well as in the design and control of thermal systems, e.g., the study of transient heat transfer phenomena associated with the reentry of spacecraft [1, 2, 3], the determination of thermophysical properties of materials [4, 5, 6], the control of solidification process [7, 8, 9, 10, 11, 12, 13], etc. The growing interest in the development and implementation of methods for solving inverse heat transfer problems is due to the fact that:

1. Advances in aeronautics, energetics, metallurgy, chemical engineering, medicine, etc. often require solutions to various thermal problems that can only be obtained by inverse methods. The need to develop reliable techniques for solving inverse heat transfer problems is thus dictated by the progresses of these advanced technologies;

2. Inverse problems are ill-posed problems and were for a long time considered to be unsolvable and therefore, of no practical interest. However, recent developments in mathematical theory have made it possible to obtain "meaningful" solutions to

various inverse problems of practical importance;

3. Methods for solving inverse problems usually require rather heavy computations, making "hand calculation" impractical, except for the most simple problems. The rapid development of computers has undoubtedly given a tremendous thrust to the advance of sophisticated inverse techniques in various engineering systems.

At present, the number of practical applications of inverse problems is increasing rapidly in the diagnostic, design and control of various systems where it is necessary to determine, from some known state of the system, the cause leading to this state, such as the thermophysical properties of the system or the thermal conditions imposed on its boundary. In other words, we have to find the cause of a given or desired state of the system. These problems are therefore referred to as inverse problems as they are posed against the causal principle of physics. Mathematically, they are considered as ill-posed problems in the sense of Hadamard [14, 15, 16].

Two typical examples of inverse heat transfer problems can be found in the early development of high-speed space craft. The first example is related to the design of thermal protection for reentry vehicles whose motion induces automatically a tremendous viscous heating by the surrounding atmosphere. The knowledge of the heat flux on the outer surface of the spacecraft is therefore crucial for the design of heat shields. The most reliable information that may lead to this knowledge are the temperature measurements performed beneath the vehicle surface. We thus have to deal with a practical heat transfer problem of determining the boundary heat flux from the measured temperatures inside a body [17, 18, 3, 19, 20, 21, 22, 23, 24, 25, 26, 27]. The second example is related to the determination of thermophysical properties of heat-protective materials to be used as heat shields for spacecraft. As measurements of thermophysical properties at very high temperatures can not be done by classical methods, the thermal conditions

under which the material will be submitted may be simulated on test stands and measurements of the resulting temperature field may be used to deduce the unknown thermophysical properties. Here, we encounter another practical inverse problem of determining some characteristic parameter of a system from the measurements of its temperature under some given thermal boundary conditions [4, 5, 6, 28]. Other typical inverse heat transfer problems consist of determining the initial temperature of a system [25], (such as the determination of the historical climate of the earth's ground layer), or the determination of the shape of a body [11], (such as the detection of a melting front in a phase change process). These problems can be referred to as retrospective inverse problems and geometric inverse problems, respectively, while the two preceding examples may be referred to as boundary condition inverse problems and parameter identification inverse problems. Classification of various inverse problems may also be done according to their practical purposes. For example, we may define such categories as inverse diagnostic problems, inverse control problems, inverse design problems, etc.

1.1 Inverse Heat Transfer Problems in Practical Applications

Inverse heat transfer problems frequently encountered in various practical applications will be described below to illustrate their importance and utility.

1. Heat measurements and thermal loading control

In heating testing of engineering systems or in situations involving the determination of temperatures, heat fluxes or heat transfer coefficients on the surface of a body, it is difficult, albeit impossible to actually measure time-dependent heat fluxes and heat transfer coefficients. The surface temperature of the system is also unaccessible for direct measurements. It is however possible to measure the temperatures within the system or at some parts of its boundary. It becomes therefore

to solve the inverse boundary condition problem, i.e. to determine the boundary conditions from the measurements of temperatures at internal points. In fact, such problems are often encountered in test gas-dynamic systems, in thermal vacuum chambers, in the course of flight simulation, in full-scale tests of flying vehicles, etc.

2. One-dimensional heat flux sensors

Among the most widely used heat flux sensors are those designed so that the temperature field in the sensor may be considered as a one-dimensional temperature field in a flat plate. Then, an inverse problem of determining the surface heat flux by measuring the temperature at some internal point of the sensor must be solved.

3. Parameter determination techniques

The determination of various temperature-dependent thermophysical parameters can be achieved by inverse techniques. For example, the convection heat transfer coefficient on a given surface and its radiative emissivity may be determined by using two sensing elements with different thermal properties, but coated with the same material (to be studied). By solving an inverse parameter problem, one can determine these parameters as functions of time. As the measured temperature of the sensor also varies with time, one can thus deduce the expressions of these parameters as functions of temperature.

4. Determination of contact thermal resistance

Contact resistances between connected parts of structures having a great number of revetted joints and hinges, or the resistances of adhesive films in multi-layer thermal shielding coatings can be successfully studied under unsteady heating conditions by solving the boundary inverse problem for specially-designed conducted experiments.

5. Determination of frictional heat generation

Inverse methods can be used to determine the heat generation during the friction between two solid bodies. Such knowledge is of importance in studies of the operating characteristics of bearings, e.g., the friction moment which is determined by the heat release intensity in the contact zone.

6. Optimization of design objectives

The design objectives of thermal systems consist of the specification of the thermal state of the desired system. The designer then have to determine the unknown parameters of the system and/or its boundary conditions to satisfy the design objectives. From a cause-effect point of view, the optimization of design objectives of thermal systems may be solved as an inverse heat transfer problem in an extremum statement. On the basis of known (permissible) thermal states, we should find the causal characteristics that would lead to these states while satisfying the optimum design criterion.

7. Control of manufacturing processes

The quality of a material or product may depend on the heat transfer history of the manufacturing process. For example, the microstructure of a metal strongly depends on the temperature gradient within the solid phase and the progression of the solid/liquid interface during the solidification process. To obtain a desired microstructure, one thus has to control the heat fluxes on both sides (solid and liquid) of the solidification front. However, these heat fluxes can only be controlled by the thermal conditions to be imposed on the boundaries of the mould. One is therefore led to an inverse boundary problem.

8. Applications in other domains

Finally it should be noted that methods for solving inverse heat transfer problems can be applied to others research fields where one has to deal with phenomena

governed by parabolic or elliptic partial differential equations., such as the case of ground water flows. Among different classes of inverse heat transfer problems (inverse parameter identification problems, inverse retrospective problems, inverse geometric problems, inverse boundary problems), let us note that inverse boundary problems belong to one of the most important and largest classes of thermal modelling problems. The resons are two-fold. First, there may be alternative to the treatment of other inverse problems. The thermophysical properties of a solid, for example, may be effectively determined by solving an inverse coefficient problem. However, they can also be determined by other methods based on the laws of stationary and quasi-stationary heat processes. Second, inverse boundary problems present a greater challenge than the other classes of inverse problems, in the sense that their solutions are more difficult to be regularized (i.e. to be stabilized with respect to random errors in the given data). Furthermore, many methods developed for solving inverse boundary problems can be applied as well to other types of inverse problems.

1.2 Review of Literature

The first attempt to solve an inverse heat transfer problem was related to the determination of the historical climate and thermal conductivity of the earth's ground layer. Stefan has obtained an infinite series solution to the inverse heat conduction in 1890 [1]. This result can be considered as the first exact solution of an inverse one-dimensional conduction problem. However, it was not well-known until Tyomkin and Burggraf [29] respectively obtained, in 1961 and 1964, similar results for similar inverse heat conduction problems. It appears that, although the formulation and solutions of inverse conduction problems were presented over a century ago, their development has rapidly grown only during the last twenty years, due to a combination of advanced technologies, new mathematical achievements and

modern computational facilities. Recent progresses in inverse heat transfer problem are attested by the appearance of the many books on this subject during the last ten years. An excellent review of literature and comprehensive bibliography can be found in the following books [30, 31, 1, 2, 32]:

1. J. V. Beck, B. Blackwell and C. R. St-Clair, Inverse Heat Conduction : Ill-Posed Problems, Wiley-Interscience, New York, 1985;

2. D. A. Murio, The Mollification Method And The Numerical Solution of Ill-Posed Problems, John Wiley, New York, 1993;

3. O. M. Alifanov, Inverse Heat Transfer Problems, Springer-Verlag, Berlin Heidelberg, 1994;

4. O. M. Alifanov, E. A. Artyukhin and S. V. Rumyantsev, Extreme Methods for Solving Ill-Posed Problems with Applications to Inverse Heat Transfer Problems, Begell House, New York, 1996;

5. E. Hensel, Inverse Theory and Applications for Engineers, Prentice Hall, Englewood Cliffs, N. Y., 1991.

We first note that the great majority of existing works were devoted to the inverse one-dimensional conduction problems (1D IHCP). Among these works, we can further find two main types of problems, namely the inverse boundary problems and the inverse parameter problems.

For the purpose of our study, we shall focus our attention on existing works related to the inverse boundary problem. We may thus cite the much-mentioned work of Burggraf [29] who presented a series solution for the boundary heat flux of a solid slab in terms of the temperature and heat flux measured on the opposite side of the slab. Also very much cited are the works of Beck et al. [30, 33,

34], Blackwell [35, 36] and Hills [37, 38, 39] on the so-called future time method to obtain smooth solutions of inverse heat conduction problems. Other workers proposed various numerical methods of solution (finite-difference space marching, finite element, boundary element) coupled with different regularization techniques (future-time, mollification, Tikhonov regularization, iterative regularization). For example, Beck et al. have used the future time technique to solve the IHCP by various numerical methods. Murio et al. [40, 41] have studied the mollification technique to be used in conjunction with the space-marching method of solution while other authors (Weber, Elden) proposed to modify the parabolic heat equation into a weakly hyperbolic equation by considering a finite (instead of an infinite) propagation velocity of heat [42]. More importantly, with the development of the space programs, much progress has been achieved by the Russian scientists in solving various inverse heat transfer problems. Starting with the pioneering works of Tikhonov [43], the regularization technique for these ill-posed problems has received a solid mathematical foundation and has been successfully applied to a wide class of inverse problems. Among the solution methods developed by the Russian scientists, one of the most versatile and robust algorithm is the iterative method of optimization by conjugate gradient technique [2, 18, 3]. This method consists essentially of casting the inverse heat conduction problem into an extremum formulation to solve iteratively by conjugate gradient technique. This iterative algorithm was found to have a very stabilizing effect against random errors in the given data. Besides the Russian school (Tikhonov, Arsenin, Shumakov, Artyukhin, Rumyantsev, Alifanov, etc. [43, 1, 44, 2, 18, 3, 19]), many workers in Germany (Gorenflo, Reinhardt, Hao [21, 22, 45, 46, 47, 15, 48, 49, 50, 51, 52, 53]) have actively contributed to the study of Tikhonov regularization as well as other techniques such as regularization by future time, mollification and hyperbolization. Generally speaking, the German works are more oriented towards the mathematical analysis of the ill-posed nature of canonical inverse problems, the Russian works were based on a solid mathematical

background and covered a great variety of practical situations. American works, such as those by Beck et al, are lighter in theory and more clearly illustrated with numerical results. Although one should ultimately need massive computational efforts to arrive at some reliable solutions for practical problems, it should be noted that hitherto inverse problems were mostly "solved" intuitively by experts, due to the lack of rational algorithms for such problems. Future works in this domain have to be devoted therefore to the development of better methods of solution as well as to the application of these methods to more complicate problems. This seems to be the trend that emerged from some recent works [54, 28, 21, 25] .

1.3 Objectives and Contents of the Thesis

Generally speaking, existing works were focused on the development of a reliable method for solving the canonical one-dimensional inverse heat conduction problem. The 2D IHCP thus remains a rather open problem, especially from a numerical approach. The purposes of this thesis are to address the following questions:

How strongly does the ill-posedness of 2D IHCP manifest in a direct approach to its solution by the space-marching method?

How efficiently does the mollification technique may regularize, i.e. to stabilize the solution against random noises?

How strongly does the ill-posedness of 2D IHCP manifest in an optimization approach to its solution by the iterative conjugate gradient method?

How efficiently does the iteration number may regularize the solution against high-frequency components of the given data in particular, and against random noises, in general?

Our main objectives are two-fold : first, to uncover the symptoms of the ill-

posedness of 2D IHCP in the two completely different methods of solution, namely the direct method by space marching and the iterative method by conjugate gradient technique. Second, to analyze the regularization mechanisms by the mollification and iteration processes, respectively. The final objective is to propose a reliable algorithm for solving a given 2D IHCP without any a priori knowledge about the given data and/or the required solution.

The main contents of this study consist of the following topics:

1. Introduction: general description of inverse heat transfer problems, review of literature and objectives of the present study;
2. Mathematical formulation of the two-dimensional inverse heat conduction problem;
3. Steady state solutions by space marching method and regularization by filtering technique;
4. Steady state solutions by optimization method and regularization by iterative conjugate gradient technique;
5. Time-dependent solutions by optimization method with conjugate gradient and filtering techniques;
6. Summary of results and concluding remarks.

The thesis is completed with a list of references that may be useful and complementary to the development of the present work.

CHAPTER II

PROBLEM FORMULATION

In solving inverse as well as direct heat transfer problems, the thermal behavior of a system has to be represented by a mathematical model. The mathematical model may be either a system of partial differential equations, or a system of ordinary differential equations. The first type is often called model with distributed parameters while the second is referred to as model with lumped parameters. The calculation of the thermal state of a real system can be considered as a mathematical simulation which is often the counter part of a more realistic simulation, namely an experimental simulation. It should be noted that by performing a mathematical simulation of a thermal system, we actually go through two levels of approximations. At first, the adopted mathematical model is necessarily a simplification of the real system, however sophisticate it may be from a mathematical point of view. Even an exact solution to this model is a mere approximate representation of the physical system under consideration. Once a mathematical model is chosen, the following step involves necessarily a second kind of approximations that are directly related to the method of solution. The validity of the desired results thus depends on both levels of approximations which have to be assessed consistently.

In this study, we are only concerned with the accuracy and stability of the solution obtained by various methods of solution for the 2D IHCP as modeled by a linear heat conduction equation.

2.1 Mathematical Model

Let us consider a two-dimensional, linear heat conduction problem in a region $\Re$. The governing heat diffusion equation is

$$\nabla \cdot k\nabla T'(r') + S'(r',t') = \frac{1}{\alpha}\frac{\partial T'}{\partial t'}. \tag{2.1}$$

where k is thermal conductivity, S' is the internal heat source term and α is the thermal diffusivity.

$$\alpha = \frac{k}{\rho c} \tag{2.2}$$

where ρ is the density and c is the specific heat. It is assumed that the material has homogeneous heat conductivity.

Three different types of boundary conditions, namely, prescribed temperature, prescribed heat flux and convection might happen along the boundaries of $\Re$. They are respectively

$$T'(r',t') = f_1(r',t'), \tag{2.3}$$

$$k\frac{\partial T'(r',t')}{\partial n} = f_2(r',t'), \tag{2.4}$$

$$k\frac{\partial T'(r',t')}{\partial n} + h(r')T'(r') = f_3(r',t') \tag{2.5}$$

where $h(r')$ is convection coefficient and $\partial/\partial n$ is the derivative along the outward normal of the boundary surface.

In well-defined problem, the temperature distribution is determined by boundary conditions specified along all the boundary surfaces. However, sometimes not all the boundaries can be measured easily. One way to deal with such a problem is getting some temperature measurements at other locations that can be easily accessible to compensate for the missing boundary condition.

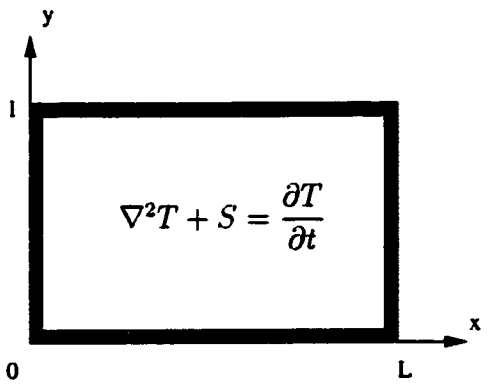

Figure 2.1: The problem geometry

In the present study, we consider a cavity $0 \leq x' \leq L_0$, $0 \leq y' \leq H_0$, as shown in Fig. 2.1.

The governing equation can be made dimensionless by the following scaling

$$\begin{cases} T = \dfrac{T'}{\Delta T'}; \\ x = \dfrac{x'}{H_0}; \\ y = \dfrac{y'}{H_0}; \\ t = \dfrac{t'}{t_f}; \\ S = \dfrac{S'}{S_f} \end{cases} \tag{2.6}$$

where

$$t_f = \frac{\rho c H_0^2}{k} \tag{2.7}$$

and

$$S_f = \frac{k\Delta T'}{H_0^2}. \tag{2.8}$$

The dimensionless governing equation is then

$$\nabla^2 T + S = \frac{\partial T}{\partial t}. \tag{2.9}$$

2.2 Direct Problem

If the boundary conditions are completely given, we are dealing with a direct problem which can be stated as follows.

Given the boundary conditions

$$\begin{cases} c_{11}T + c_{12}\dfrac{\partial T}{\partial x} + c_{13} = 0 \quad at \quad x = 0; \\ c_{21}T + c_{22}\dfrac{\partial T}{\partial x} + c_{23} = 0 \quad at \quad x = L; \\ c_{31}T + c_{32}\dfrac{\partial T}{\partial y} + c_{33} = 0 \quad at \quad y = 0; \\ c_{41}T + c_{42}\dfrac{\partial T}{\partial y} + c_{43} = 0 \quad at \quad y = 1 \end{cases} \tag{2.10}$$

where array c are coefficients which are functions of x, y and t, and the initial condition

$$T = T_0(x, y) \quad at \quad t = 0, \tag{2.11}$$

determine the temperature distribution $T(x, y, t)$ in the cavity region $0 \leq x \leq L$, $0 \leq y \leq 1$ during the period $0 \leq t \leq t_{max}$ satisfying Eq. 2.9.

2.3 Inverse Problem

Suppose that the measurements of both the temperature $T(y, t)$ and heat flux $\partial T/\partial x$ at one vertical boundary are provided, but no information is available about the boundary condition at the other vertical boundary. The objective then is to solve Eq. 2.9 under the boundary conditions

$$\begin{cases} T = F_0(y,t) & at \quad x = 0; \\ \dfrac{\partial T}{\partial x} = G_0(y,t) & at \quad x = 0; \\ c_{11}T + c_{12}\dfrac{\partial T}{\partial y} + c_{13} = 0 & at \quad y = 0; \\ c_{21}T + c_{22}\dfrac{\partial T}{\partial y} + c_{23} = 0 & at \quad y = 1 \end{cases} \tag{2.12}$$

where F_0 and G_0, namely the Cauchy data, are given functions of y and t.

This is a two-dimensional inverse heat conduction problem and will be referred to as a 2D IHCP. To solve this problem, we focus our attention on two principal approaches, namely the direct method by space marching and the iterative method by conjugate gradient technique. These, as we will see, may be considered as two complementary approaches to the IHCP, to be applied according to the specific application under consideration. In fact, when used in conjunction with an appropriate mollification technique, the space marching technique is very fast to provide a regularized albeit distorted solution, while the iterative conjugate gradient technique proves to be slow, but robust and more reliable. A detailed study of each method will be reported in the following chapters, respectively.

CHAPTER III

THE MARCHING METHOD AND REGULARIZED SOLUTIONS

Space marching schemes have been a mainstay in the numerical computation of direct problems (Roache [55]). A description of these schemes to inverse heat conduction problem was given in a paper by Carasso [42].It was shown that for ill-posed initial value problems, all consistent marching schemes are unconditionally unstable, and marching algorithms can thus "blow up" at widely different rates as Δt, Δx are decreased. Various methods were proposed to stabilize the solutions against the amplification of measurement and computation errors. One technique that has been extensively used with the marching method consists of using a low-pass filter to eliminate the high-frequency components in the random noises of the measured data and/or the round-off errors in numerical computations. Such technique has been referred to as "mollification method", and studied by Murio and collaborators [6, 56, 31, 40], as well as by Hao [51]. These authors have analyzed the basic question of errors bound in terms of the so-called mollification kernel and mollification parameter. The technique was mostly applied to 1D IHCP. Two difficulties are encountered in the implementation of this technique. First, the mollification

of the end points must be done with an extrapolation of the data. Second, the repeated application of the mollification may successfully eliminate high frequency noises and/or computational round-off errors, but also significantly distort the final result. The choice of an optimum mollification parameter, of a realistic extrapolation of the given data, and of a minimum necessary number of applications, must be based on some a priori knowledge of the unknown function and of the numerical computations.

In this chapter we will solve the 2D steady IHCP by the space marching method. We will first describe the marching process and its implementation, and consider next the amplification of errors in the marching direction: Both errors due to measurements and errors due to numerical truncations will be studied in details.

After showing how high-frequency errors may be amplified during the marching process, we will study three different types of filter to stabilize the solutions against these errors by eliminating their high-frequency components.

In each case considered, the numerical results obtained by space marching method will be compared with the analytical solutions in order to show:

1. The unstable nature of the problem against either numerical and/or experimental errors;

2. The efficiency of the filtering technique using different types of filter to obtain solutions that are stable against the above-mentioned errors.

The chapter will close with a summary of the results obtained, and a recommendation for the implementation of a stable marching technique to solve the 2D

IHCP.

3.1 The Marching Method

To study the space marching method in solving the steady inverse conduction problem, let consider the steady state conduction equation

$$\nabla^2 T = -S \tag{3.1}$$

with the boundary conditions

$$\begin{cases} T = F_0(y) & at \quad x = 0; \\ \dfrac{\partial T}{\partial x} = G_0(y) & at \quad x = 0; \\ c_{11}T + c_{12}\dfrac{\partial T}{\partial y} + c_{13} = 0 & at \quad y = 0; \\ c_{21}T + c_{22}\dfrac{\partial T}{\partial y} + c_{23} = 0 & at \quad y = 1 \end{cases} \tag{3.2}$$

where F_0 and G_0, namely the Cauchy data, are given functions of y.

Space marching method consists of solving the above equation as an initial-value problem. For direct problem the basic idea of marching method is guessing the missing conditions of a boundary value problem at one boundary and marching from this boundary to a second boundary as an initial-value problem [55]. The resulting values at the second boundary are then compared with the given boundary values, and on that basis the guessed conditions are corrected and the march is repeated for the final correct solution. The correction for linear equations can be exact and only two marches are required to obtain the solution. For nonlinear equations, the corrections are approximate and the marching has to be used iteratively.

For the inverse problem considered here, the marching method can be naturally adapted since two conditions at one boundary are available and no guessing of the

initial condition is needed. Only one march is enough to obtain the solution.

3.1.1 The Discretized Equations

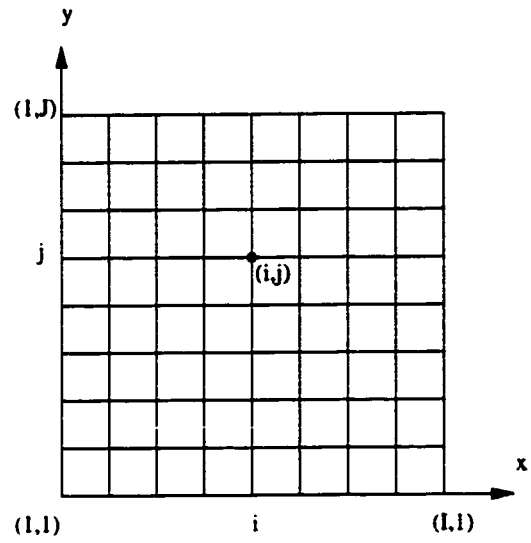

Figure 3.1: The grid system of the problem

In the finite-difference approach, the domain is discretized so that the dependent variables are considered only at discrete points. The two-dimensional grid system used in this problem is shown in Fig. 3.1, where (i, j) is the grid point in rectangle coordinate. Derivatives are approximated by differences resulting in an algebraic representation of the partial differential equation (PDE). The nature of the resulting system of algebraic equations depends on the character of the problem posed by the original PDE (or system of PDEs).

In this study, the control-volume formulation described by Patankar [57] is used to obtain the discretization equations.

For any grid P of the system, Eq. 3.1 has the discretized form

$$a_P T_P = a_E T_E + a_W T_W + a_N T_N + a_S T_S + b \tag{3.3}$$

where a_W, a_E, a_S, a_N, a_P and b are the coefficients varying with the position of the node.

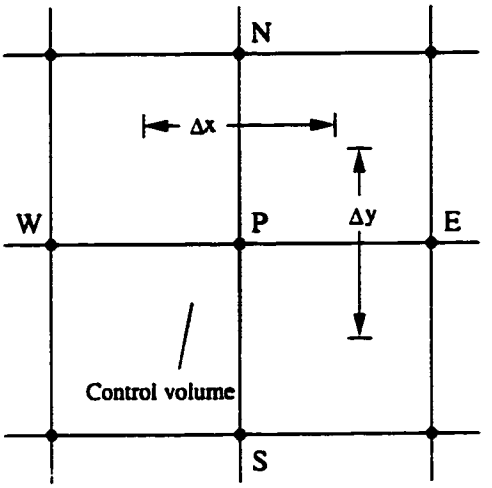

Figure 3.2: Control volume for internal node

For internal nodes shown by Fig. 3.2

$$\begin{cases} a_E &= \dfrac{\Delta y}{\Delta x} = a_W; \\ a_N &= \dfrac{\Delta x}{\Delta y} = a_S; \\ a_P &= 2(\dfrac{\Delta y}{\Delta x} + \dfrac{\Delta x}{\Delta y}); \\ b &= S_P \Delta x \Delta y. \end{cases} \tag{3.4}$$

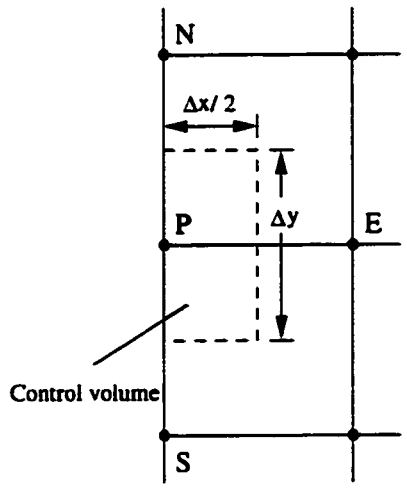

Figure 3.3: Control volume for boundary node

The nodes along the boundaries have different kind of control volumes. Fig.

3.3 is the control volume for the west boundary node. The coefficients are

$$\begin{cases} a_W &= 0; \\ a_E &= \dfrac{\Delta y}{\Delta x}; \\ a_S &= \dfrac{1}{2}\dfrac{\Delta x}{\Delta y} = a_N; \\ a_P &= \dfrac{\Delta y}{\Delta x} + \dfrac{\Delta x}{\Delta y}; \\ b &= S_P \dfrac{\Delta x \Delta y}{2} - G_{0P}\Delta y. \end{cases} \tag{3.5}$$

When $c_{12} = 0$ and $c_{22} = 0$, which means the south and north boundary conditions are given boundary temperature, the equations give directly

$$\begin{cases} T_P &= -\dfrac{c_{13}}{c_{11}}; \qquad (South) \\ T_P &= -\dfrac{c_{23}}{c_{21}}. \qquad (North) \end{cases} \tag{3.6}$$

Otherwise the coefficients are respectively

$$\begin{cases} a_W &= \dfrac{1}{2}\dfrac{\Delta y}{\Delta x} = a_E; \\ a_S &= 0; \\ a_N &= \dfrac{\Delta x}{\Delta y}; \\ a_P &= \dfrac{\Delta y}{\Delta x} + \dfrac{\Delta x}{\Delta y} - \dfrac{c_{11}}{c_{12}}\Delta x; \\ b &= S_P \dfrac{\Delta x \Delta y}{2} + \dfrac{c_{13}}{c_{12}}\Delta x, \end{cases} \tag{3.7}$$

and

$$\begin{cases} a_W &= \dfrac{1}{2}\dfrac{\Delta y}{\Delta x} = a_E; \\ a_S &= \dfrac{\Delta x}{\Delta y}; \\ a_N &= 0; \\ a_P &= \dfrac{\Delta y}{\Delta x} + \dfrac{\Delta x}{\Delta y} + \dfrac{c_{21}}{c_{22}}\Delta x; \\ b &= S_P\dfrac{\Delta x \Delta y}{2} - \dfrac{c_{23}}{c_{22}}\Delta x. \end{cases} \tag{3.8}$$

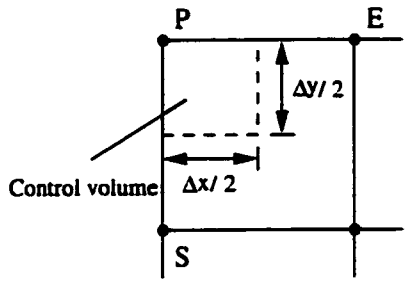

Figure 3.4: Control volume for corner node

When the south and north boundary temperatures are unknown, the south-west and north-west corners (Fig. 3.4) have to be considered separately. For the

south-west corner

$$\begin{cases} a_W &= 0; \\ a_E &= \dfrac{\Delta y}{\Delta x}; \\ a_S &= 0; \\ a_N &= \dfrac{\Delta x}{\Delta y}; \\ a_P &= \dfrac{\Delta y}{\Delta x} + \dfrac{\Delta x}{\Delta y} - \dfrac{c_{11}}{c_{12}}\Delta x; \\ b &= S_P \dfrac{\Delta x \Delta y}{2} + \dfrac{c_{33}}{c_{32}}\Delta x - G_{0P}\Delta y. \end{cases} \tag{3.9}$$

For the north-west corner

$$\begin{cases} a_W &= 0; \\ a_E &= \dfrac{\Delta y}{\Delta x}; \\ a_S &= \dfrac{\Delta x}{\Delta y}; \\ a_N &= 0; \\ a_P &= \dfrac{\Delta y}{\Delta x} + \dfrac{\Delta x}{\Delta y} + \dfrac{c_{21}}{c_{22}}\Delta x; \\ b &= S_P \dfrac{\Delta x \Delta y}{2} - \dfrac{c_{23}}{c_{22}}\Delta x - G_{0P}\Delta y. \end{cases} \tag{3.10}$$

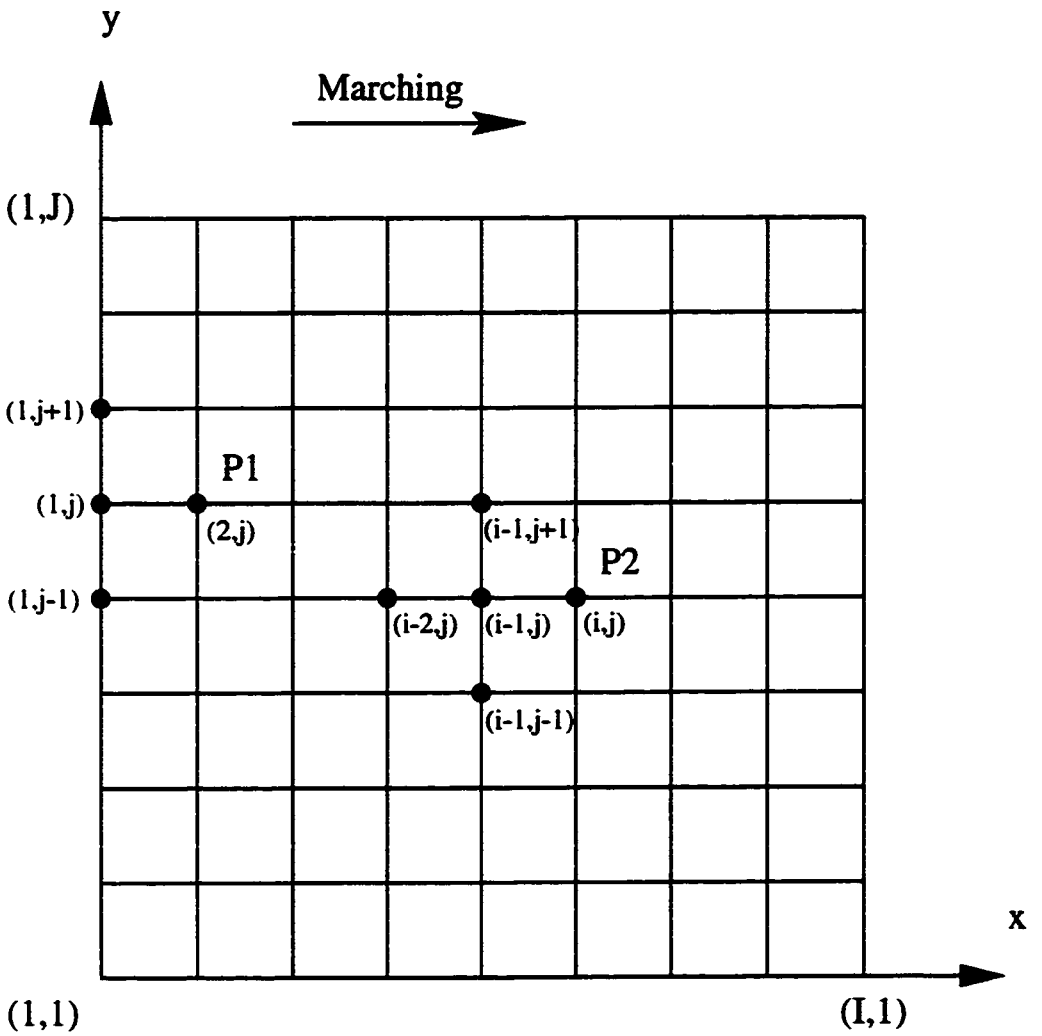

Figure 3.5: Marching process

3.1.2 The Marching Process

The marching process of the present problem is shown by Fig. 3.5. Starting with given values of T and $\partial T/\partial x$ at $x = 0$, i.e. for $i = 1$, $1 \leq j \leq J$, we can march in the x-direction to obtain successively the values of $T_{i,j}$ for $2 \leq i \leq I$, $1 \leq j \leq J$. According to Eq. 3.3, the marching equation is

$$T_E = (a_P T_P - a_W T_W - a_N T_N - a_S T_S - b)/a_E \tag{3.11}$$

which can be turned into

$$T_{i,j} = (a_P T_{i-1,j} - a_W T_{i-2,j} - a_N T_{i-1,j+1} - a_S T_{i-1,j-1} - b)/a_E \tag{3.12}$$

where a_W, a_E, a_S, a_N, a_P and b are the coefficients of the discretization equation of node $(i-1, j)$. Now that the coefficients vary with node position as expressed above, the marching equation varies too. For example, as shown in Fig. 3.5, T_{P1} is calculated from $T_{1,j}$, $T_{1,j+1}$, $T_{1,j-1}$ and heat flux at $(1, j)$ while T_{P2} results from $T_{i-1,j}$, $T_{i-1,j+1}$, $T_{i-1,j-1}$ and $T_{i-2,j}$.

3.1.3 Error Propagation in Marching Method

As described, the marching method is a very simple direct method to solve the inverse conduction problem. It is however unstable because of the error propagation in the marching direction.

It can be shown that in solving the Poisson's equation by marching method, if one starts the marching process with a boundary condition having very small errors, the solution may diverge from the exact solution while advancing in the marching direction [55].

For concreteness, consider direct problem with Dirichlet boundary conditions at all boundaries. Suppose the value vector $T'_{2,j}$ is in error by the error vector $\epsilon_{2,j}$,

i.e.

$$T_{2,j} = T'_{2,j} + e_{2,j}. \tag{3.13}$$

As known in §2.2, for internal node (i,j),

$$\frac{T_{i+1,j} - 2T_{i,j} + T_{i-1,j}}{\Delta x^2} + \frac{T_{i,j+1} - 2T_{i,j} + T_{i,j-1}}{\Delta y^2} = S_{i,j}. \tag{3.14}$$

Then the remaining temperature values for $2 \leq i \leq I$ and $2 \leq j \leq J-1$ are calculated in one march, starting at $T_{3,j}$, by rearrangement of Eq. 3.14,

$$T'_{i+1,j} = \Delta x^2 S_{i,j} + (2+2\alpha)T'_{i,j} - \alpha(T'_{i,j+1} + T'_{i,j-1}) - T'_{i-1,j} \tag{3.15}$$

where $\alpha = (\Delta x/\Delta y)^2$. The error propagation equation is thus

$$e_{i+1,j} = (2+2\alpha)e_{i,j} - \alpha(e_{i,j+1} + e_{i,j-1}) - e_{i-1,j} \tag{3.16}$$

with boundary values along west, south and north boundary of

$$e_{1,j} = e_{i,1} = e_{i,J} = 0. \tag{3.17}$$

There is a linear relation between the final error of $e_{I,j}$ and initial error $e_{2,j}$

$$E_I = C E_2 \tag{3.18}$$

where $E_2 = e_{2,j}$, $E_I = e_{I,j}$ and C is the influence coefficient matrix.

For one-dimensional problem, the error propagation is linear in i. But for multidimensional problems the error may propagate exponentially. Roache [55] indicated that the leading term of $e_{i,jc}$ at the center of the mesh $(jc = (J+1)/2)$ may be $[2(1+\alpha)]^{i-2}$.

In solving inverse problems, the errors in the given boundary conditions may be due to measurements errors, or if they are simulated numerically, they may suffer from the machine round-off error. The solution away from the starting boundary is

thus sensitive to infinitesimal perturbations or errors in initial data, i.e. the error propagation becomes more significant when J gets large. A significant factor in the error propagation is from the mesh aspect ratio $\beta = \Delta x/\Delta y$. As stated above, the leading term of $e_{I,jc}$ is $[2(1+\alpha)]^{I-2}$, where $\alpha = \beta^2$. It appears that if smaller β is used, the solution will be better.

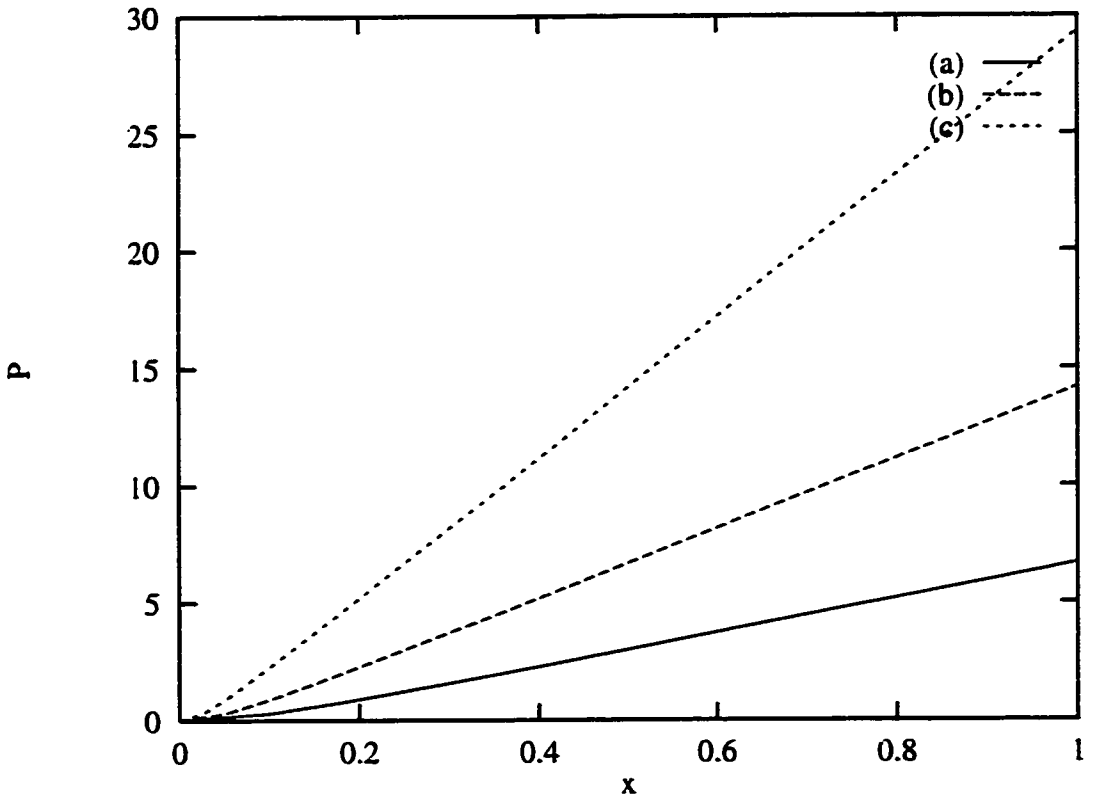

Figure 3.6: The error propagations with different mesh sizes: (a) 11×11, (b) 21×21, (c) 41×41

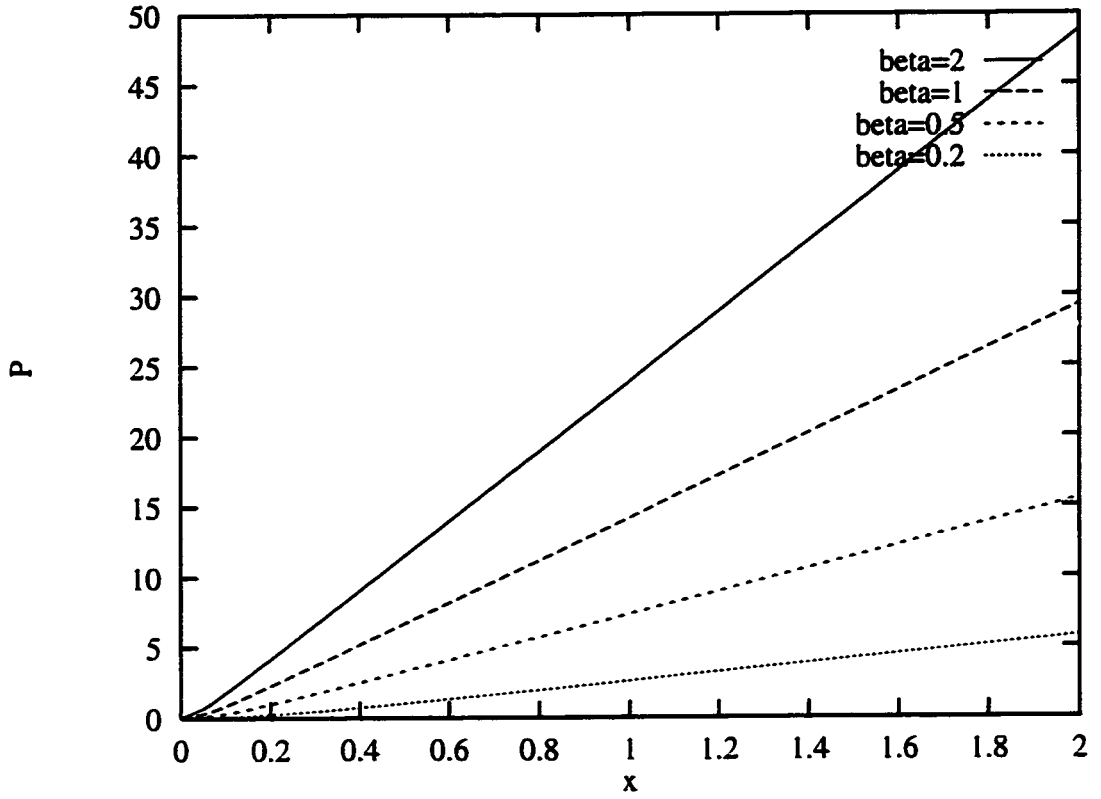

Figure 3.7: The effect of various aspect ratios on error propagation:(a) $\beta = 2$, (b) $\beta = 1$, (c) $\beta = 0.5$, (d) $\beta = 0.2$

To demonstrate the properties of the error propagation of the inverse problem for the Poisson's equation, some numerical experiments are made for the error propagations of one unit error at $(1, jc)$ along the marching direction, using different meshes. The Dirichlet boundary conditions are adopted at the south and north boundary, with $T_{i,1}$ and $T_{i,J}$ specified. Errors are evaluated as $P = log_{10}(e_{i,jc})$.

Fig. 3.6 shows the error propagations in the domain ($L = 1$) with different mesh sizes. As can be seen from this figure, the error grows much faster when J

and I increase. The problem is said to be more unstable.

The effect of mesh aspect ratio β is demonstated by Fig. 3.7. The cases are the error propagations in the domain ($L = 2$) with $\Delta x = 0.05$ and various values of Δy. Let S be the number of the significant decimal figures in machine's floating point operation. In the IBM Power Station that is used in this study $S \approx 15.95$ for double precision. To obtain solution with A significant figures requires $P \leq S - A$. Fig. 3.7 shows that mesh with smaller aspect ratio β can predict more far away.

An empirical equation to predict I_{max}, the maximum mesh size in the marching direction, is given by Roache [55] as

$$I_{max} \approx 4 + (CP - A)\beta \tag{3.19}$$

where A is required accuracy and CP is a computer parameter that depends on the word length S. It is tested to be true for the present inverse problems.

3.2 Regularized Solutions

As shown above, the marching method works when appropriate mesh size and aspect ratio are used. But in practical applications errors of measurement are unavoidable. Even when good mesh are used, the error at the measured boundary will still grow significantly to destabilize the solution. Take the case of Fig. 3.7, when $\beta = 0.2$, one unit error leads to 10^6 unit error at boundary $x = 2$. If exact boundary conditions are given at the measured boundary, i.e. error is just the machine round off error, say, 10^{-16}, the error at $x = 2$ is only 10^{-10}. This is much more than necessary. However, using the same mesh and the boundary condition with measurement errors of $O(10^{-3})$, the solution diverge long before $x = 1$. The measurement error is too large to the sensitivity of the problem. This is why the marching method is often dismissed as "useless".

In fact, the instability of this method simply reflects the ill-posedness of the inverse problem considered here. In order to treat this ill-posedness, Tikhonov's regularization technique may be applied to control the smoothness of the solution. Such regularization was shown to be equivalent to subjecting the noisy data to a low-pass filter in the Fourier-transform domain. This latter technique will be used here via the so-called mollification method with three different kernels, namely the Gaussian kernel

$$K_G = \frac{1}{\pi\delta} e^{-\frac{y^2}{\delta^2}}, \tag{3.20}$$

the Dirichlet kernel

$$K_D = \frac{1}{\pi} \frac{sinx/\delta}{x}, \tag{3.21}$$

and the Square kernel

$$K_S = \begin{cases} 1/2\delta & \text{if} \quad |x| < \delta; \\ 0 & \text{if} \quad |x| > \delta. \end{cases} \tag{3.22}$$

The mollification of the data $F(y)$ is defined as

$$F^{\bullet} = \int_{-\infty}^{\infty} K(y')F(y-y')dy'. \tag{3.23}$$

3.2.1 The Properties of the Mollification Kernels

The premise of data smoothing is that one is measuring a variable that is slowly varying but corrupted by random noise which has high-frequency components. This is why the low-pass filters are used here. They replace each data point by some kind of local average of surrounding data points. Since nearby points measure very nearly the same underlying value, averaging can reduce the level of noise without much biasing the value obtained except when stiff functions are involved.

The smoothing of data still lies in a murky area [58, 31]. Various kinds of low-pass filters are introduced for data smoothing. It is found that no one filter is very well adapted for all cases. Whether a filter works depends on to which kind of function it is applied.

To study the effect of different types of filter, three mollification kernels are studied by applying them to two functions

$$1) \quad T = -y^2$$
$$2) \quad T = sin(\pi y)$$

with random noise $0.05rand$ or single high-frequency component $0.05sin(24\pi y)$ where *rand* is a random number in $[-0.5, 0.5]$.

From the figures for various cases listed in the next pages, one can see that:

1) (Fig. 3.8) For the test function $-y^2$ with random noise, the Gaussian filter and Square filter can well smooth the noise. The result of the Dirichlet filter has some low frequency oscillations. This is because the Dirichlet filter is so sensitive to high frequency that it also eliminates the the high frequency components of $-y^2$.

2) (Fig. 3.9) For the function $sin(\pi y)$ with random noise, all three filters are fine. Since the function has only a single low frequency, the Dirichlet filter also works well.

3) (Fig. 3.10) For the function $-y^2$ with sinusoidal noise, the Gaussian filter is still good. The Square filter appears to be unable to deal with this kind of noise by simply averaging local data. The action of the Dirichlet filter is the same as that with random noise: it smoothed out the high frequency components of both the noise and the function itself.

4) (Fig. 3.11) For the function $sin(\pi y)$ with sinusoidal noise, the Gaussian filter and

the Dirichlet filter have good results while the Square filter turns out to be bad for this noise again.

These cases clearly show that

1) The Square filter is not good for the sinusoidal noise;

2) The Dirichlet filter is very powerful to eliminate high frequencies. It should be applied only to functions that have no high frequencies, otherwise the functions themselves will be strongly distorted;

3) The Gaussian filter is the one that works relatively well for all cases.

Another important thing to be noted is that although a good filter can effectively reduce the level of noise , it can deform the function significantly if applied too many times. Fig. 3.12 and Fig. 3.13 illustrate the point. The Gaussian filter and the Dirichlet filter are respectively applied to the function $-y^2$ and $sin(\pi y)$ (without noise) 20, 60 and 100 times.

3.2.2 Analysis of the Regularized Solutions

The last section shows that the Gaussian filter is suitable for all the cases tested. For the purpose of this section, only this filter will be used in the oncoming experiments.

The objective is to see whether the mollification method can successfully predict the temperature field from the Cauchy data in spite of the ill-posedness of inverse problem.

For generality, the following three cases will be examined:

1) Solution: $T = x + y$

Boundary Conditions:

$$\begin{cases} F_0(y) = y & at \quad x = 0 \\ G_0(y) = 1 & at \quad x = 0 \\ T = x & at \quad y = 0 \\ T = x + 1 & at \quad y = 1 \end{cases} \tag{3.24}$$

2) Solution: $T = x^2 - y^2$

Boundary Conditions:

$$\begin{cases} F_0(y) = -y^2 & at \quad x = 0 \\ G_0(y) = 0 & at \quad x = 0 \\ T = x^2 & at \quad y = 0 \\ T = x^2 - 1 & at \quad y = 1 \end{cases} \tag{3.25}$$

3) Solution: $T = cos(\pi x)sin(\pi y)$

Boundary Conditions:

$$\begin{cases} F_0(y) = sin(\pi y) & at \quad x = 0 \\ G_0(y) = 0 & at \quad x = 0 \\ T = 0 & at \quad y = 0 \\ T = 0 & at \quad y = 1 \end{cases} \tag{3.26}$$

The computing domain is $L = 1$.

Case 1. and Case 2.: These solutions are of first and second order, respectively, which can be represented exactly by the second order discretization scheme used presently. But because of the error propagation, one can't get solution of the same precision as in direct problem.

Firstly, to demonstrate the dependence of the solution on the mesh ratio in §2.3.2, solutions obtained by different mesh sizes are shown in Fig. 3.14 (11 × 11), Fig. 3.15 (24 × 24) and Fig. 3.16 (41 × 11). One can see that these results are consistent to Fig. 3.6 and Fig. 3.7. When suitable mesh size and aspect ratio are used, sufficiently accurate solution as shown in Fig. 3.16 can be obtained. But this is based on the exact boundary conditions.

When random noise $0.001rand$ is added to the given data F_0 for the three cases, the solutions (Fig. 3.17) are clearly unacceptable even with a 11 × 11 mesh. If the Gaussian filter is now applied at every step of marching process, the solution becomes reasonable but loses some accuracy. That is the trade-off of the regularization method. As discussed in the previous section, the filters not only reduce the level of noise in the data, but also distorts the real data. If a filter is applied too many times, the deformation of the solution become very significant to make the solution unrealistic. Fig. 3.19 is an example of solutions obtained by a 21 × 21 mesh and

by applying the Gaussian filter at every step. Case 1 is an exception because the solution $T = x + y$ is a linear function which remains unaffected by the filters.

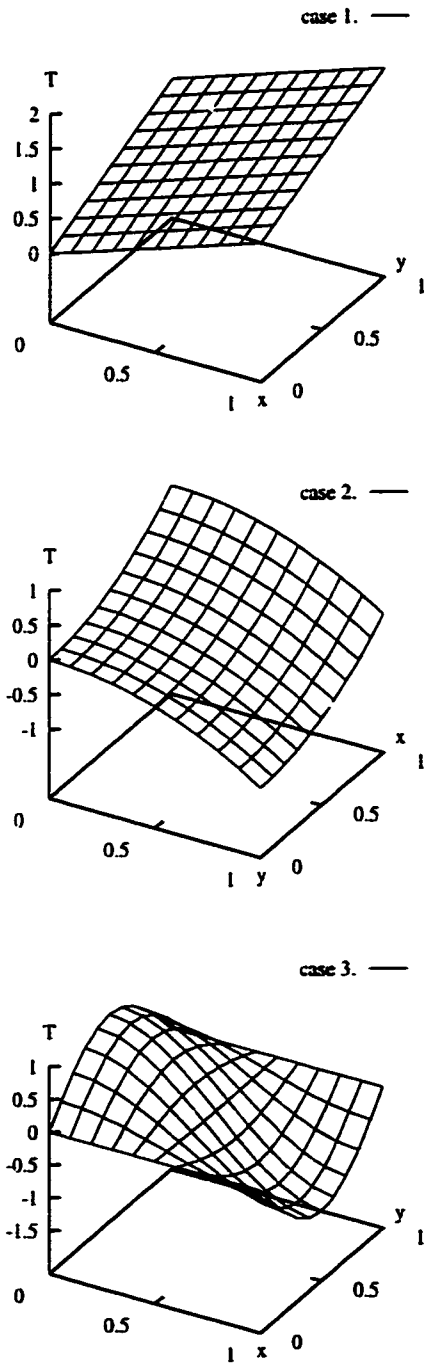

Figure 3.14: Solutions with exact measured boundary conditions (mesh size: 11×11)

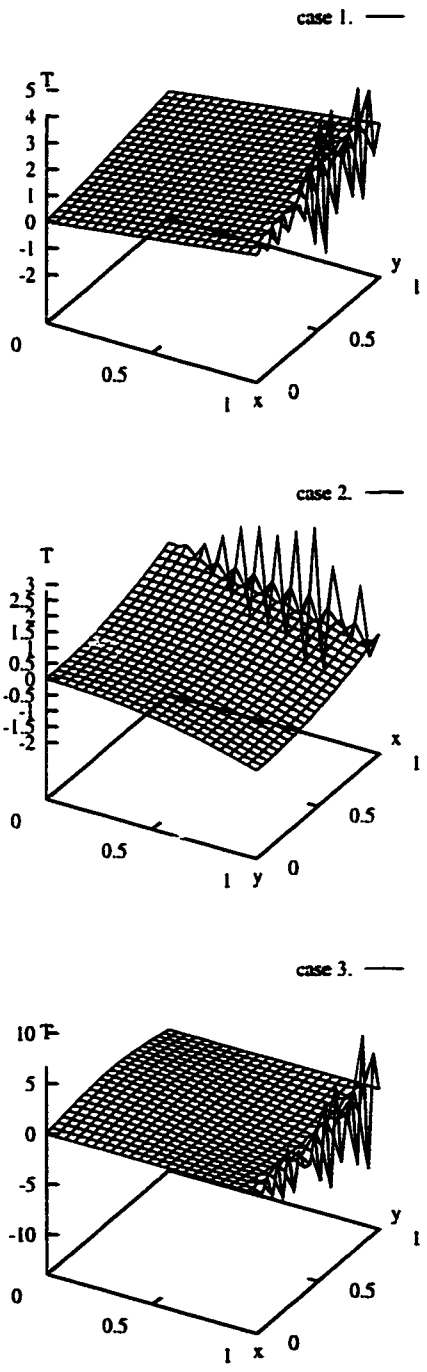

Figure 3.15: Solutions with exact measured boundary conditions (mesh size: 24×24)

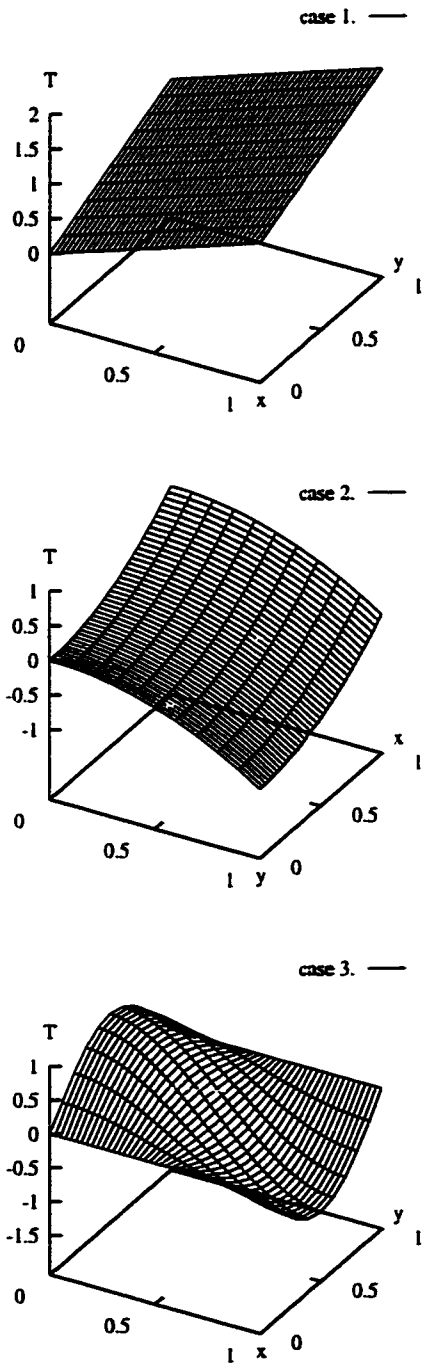

Figure 3.16: Solutions with exact measured boundary conditions (mesh size: 41×11)

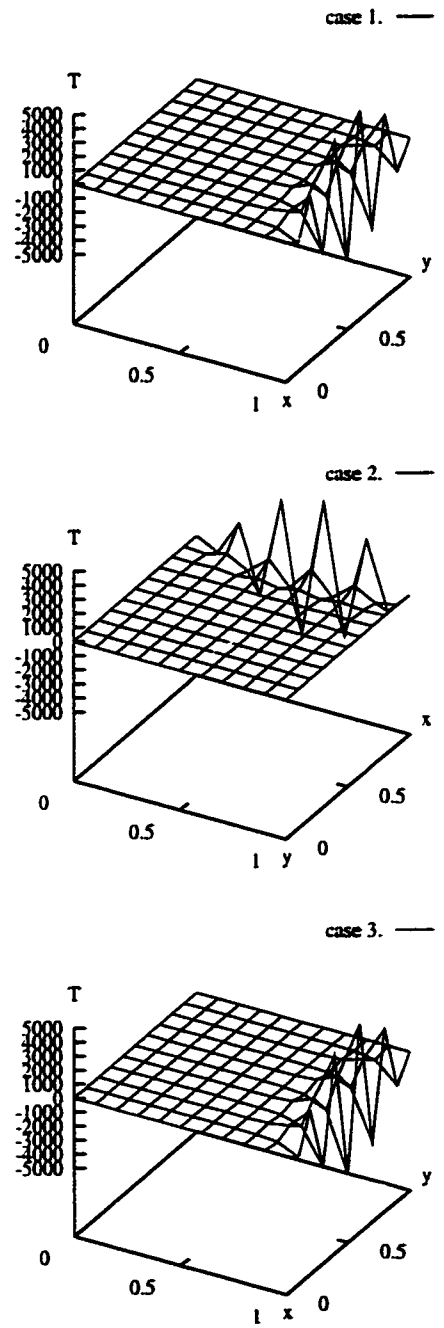

Figure 3.17: Solutions with inexact measured boundary conditions (mesh size: 11 × 11)

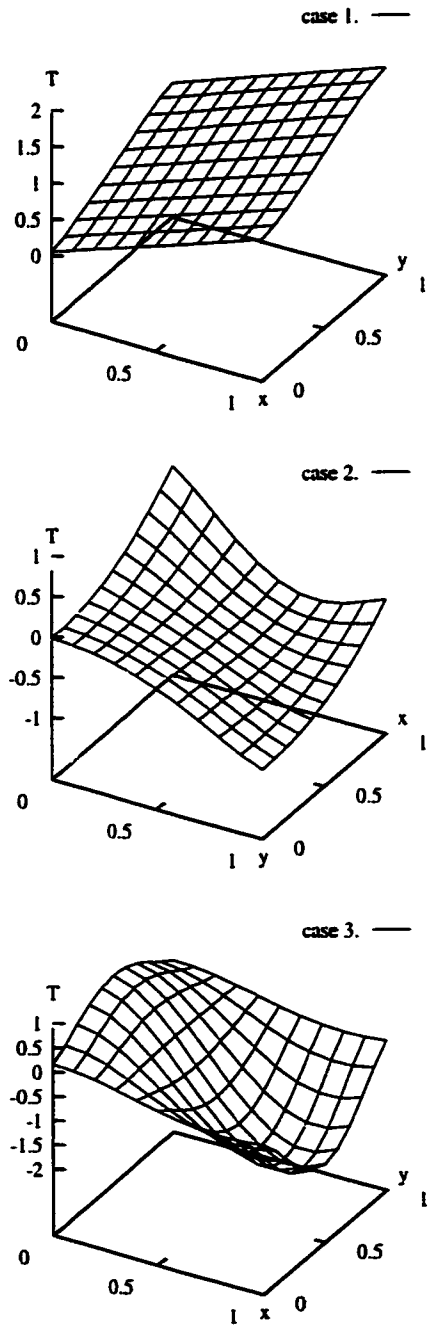

Figure 3.18: Solutions with inexact measured boundary conditions and smoothed by the Gaussian filter at every step (mesh size: 11×11)

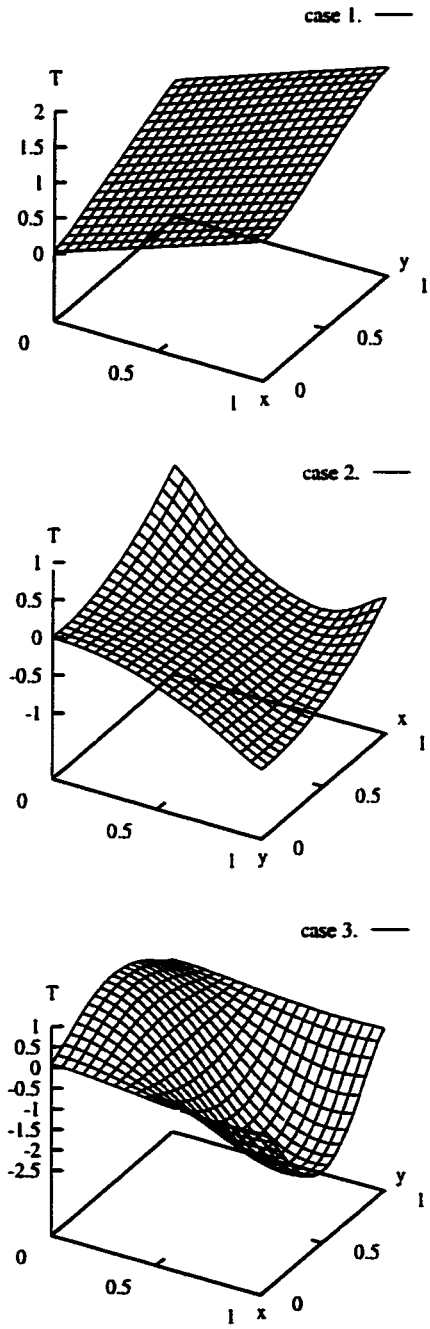

Figure 3.19: Solutions with inexact measured boundary conditions and smoothed by the Gaussian filter at every step (mesh size: 21 × 21)

3.3 Concluding Remarks

In this chapter we have presented the space marching technique in conjunction with the mollification method to solve the 2D IHCP.

It appears that the space marching technique may be naturally adapted to, as if it was in fact made for, the inverse problem with Cauchy data: It is easy to understand, simple to implement, and fast to give an answer. From a practical point of view, it is therefore a desired method for solving engineering problem in the real-time mode.

Its drawback is closely related to the ill-posed nature of the IHCP itself, i.e., it is very unstable against high-frequency errors of the given data. These errors may arise either from the measured experimental data and/or the round-off errors of numerical computations during the marching process. In order to stabilize the solution, we have studied three different types of low-pass filters to be used in the so-called mollification method. By applying these filters to the temperature distribution (along the y-direction) at each step during the marching process (along the x-direction), we have succeeded in obtaining smooth (i.e. stable) solutions. Unfortunately, the price of such a smoothing technique is a great loss of accuracy such that the final solution may become quite unrealistic if the filter is applied too many times during the marching process. An optimum strategy may be therefore based on a "good" combination of mollification factor and grid size.

Overall, it appears that the marching technique in conjunction with the mollification method may be recommended for obtaining a rough estimation of the boundary condition in 2D IHCP if real-time solution is required for some practical reasons.

CHAPTER IV

THE OPTIMIZATION METHOD WITH CONJUGATE TECHNIQUE

Besides the space marching method described in the preceeding chapter, the function specification and the gradient method have received the most attention to deal with the ill-posed inverse problems. Function specification assumes a functional form for the heat flux over a future time interval (Beck et al. [30, 19, 33]). Specification of a funtional form over the future time provides regularization to stabilize the ill-conditioned problem (Lamm [59]). This method solves the problem in a sequential manner. Several authors have used this method to solve 2D inverse problems. Osman and Beck [54, 28] solved the space and time dependent heat transfer coefficient and the surface heat flux. Zabaras et al. [7, 8] used this method in conjuction with the boundary and finite element methods. Hsu et al. [20] applied a finite element method to the general 2D problem with inverse methods similar to functional specification.

Gradient methods, which typically apply a conjugate gradient iterative scheme, coupled iterative or Tikhonov regularization to stabilize the solution and solve the

multi-dimensional pproblem. Iterative regularization (Alifanov [1] and Alifanov et al. [2]) depends on the slowness or "viscosity" of the solution and uses the iteration index as the regularization parameter. Alifanov and Kerov [3] and Alifanov and Egorov [18] used iterative regularization, while Zabaras and Yang [9, 10], Reinhardt [21, 22] and Jarny et al. [60] used gradient methods, but not iterative regularization.

Functional specification and gradient methods are powerful approaches to solve the multidimensional IHCP. An advantage of the functional specification method is that the problem retains the causal nature, represent with a Voltera operator [59] and can be solved sequentially and implemented in an on-line procedure with possible savings in computational time and memory. On the contrary, the gradient method has to be applied on the whole time domain, and does not take advantage of the causal nature of the problem, but proves to be very robust and can be applied to a wide range of problems. Some authors therefore suggested that a sequential implementation of gradient method would be a powerful combination: the method will not require a prescribed functional form, which is particularly useful for the computational aspects of sequential implementation. See, for exemple, Beck and Murio [34], Reinhardt and Hao [21] and Artyuhkin and Gedzhadze [19]. These authors have addressed the 1D IHCP to provide insight to the method. Osman et al. [54] considered for the first time a 2D implementation of sequential conjugate gradient method. Issues related to the influence of the number of future time steps and the computational requirements for a sequential implementation are largely open questions to be considered. In the present study, attention is focused on the the gradient method for IHCP as considered by Alifanov and Artyukhin et al. [2]. To compensate for the unknown boundary condition, temperature measurements T_m are provided either at the surface or at the interior points of the body. The analysis is developed for continuous measurements in space and time. The objective is to estimate $q(r,t)$ based on the given measured temperatures T_m. Hence, the

heat flux $q(r,t)$ is estimated such that the calculated temperatures T are equal to the given temperatures T_m. Due to the ill-posedness of the problem, the matching is to be satisfied in a least square sense by minimizing the objective functional E. Schemes to minimize this functional, which use iterative methods such as steepest descent or conjugate gradient, require the gradient of $E(q)$. Methods to compute this gradient depend on the function space to which $q(r,t)$ is assumed to belong. Two possibilities are a finite-dimensional space and an infinite-dimensional space. For this latter case, a priori information is not required concerning the unknown function $q(r,t)$. However, computations of the gradient then require solving an additional so-called adjoint problem. For the case where a priori information is available on the heat flux $q(r,t)$. the problem can be made finite-dimensional and the gradient can be determined by standard differential calculus. The approach considered here is the general case of infinite-dimensional problem. The unknown heat flux is assumed to be in the L^2 space of square integrable functions, with the scalar product defined by

$$(f,g) = \int fg\, drdt \tag{4.1}$$

The associated norm of a function $f(r,t)$ is

$$\| f \|^2 = \int |f(r,t)|^2\, drdt \tag{4.2}$$

Note that the solution for a finite dimensional space may be obtained as a special case of the more general infinite-dimensional case.

The algorithm of solution by conjugate gradient is described in details by Jarny et al. [60] for muli-dimensional IHCP. Numerically solving the IHCP by gradient method requires the solutions of three partial differential equations representing the direct, adjoint and sensitivity problems which are of a same type and can be solved by the same numerical method. In this study, a numerical solution is obtained by using a finite control volume approach to derive the discretized equations. (it is

worth noting that as the coefficient matrices are the same for three problems and require computations only once for constant thermal properties, direct inversion of these matrices may greatly save computation time).

4.1 Optimization Problem Formulation

The mathematical formulation of steady inverse problem has been presented in Chapter III. However, from the optimization point of view, it can be described as follows.

Suppose that to compensate for the unknown boundary condition, there are K sensors located at the positions

$$r = r_k, \qquad r_k \in \Re \tag{4.3}$$

with temperatures denoted by T_{mk}.

Also denote the unknown boundary condition by $H(r)$, and its estimated value by $H_{est}(r)$. $H(r)$ can be any one of the following quantities:

$$H(r) = f_1(r) = T(r); \tag{4.4}$$

$$H(r) = f_2(r) = k(r)\frac{\partial T(r)}{\partial n}; \tag{4.5}$$

$$H(r) = f_3(r) = k(r)\frac{\partial T(r)}{\partial n} + h(r)T(r). \tag{4.6}$$

Let $T(r, H)$ denote the solution of the direct problem obtained with the known boundary conditions and $H(r)$. Then the objective of the optimization is to find a $H(r)$ such that

$$T(r_k, H) = T_{mk} \tag{4.7}$$

for $k = 1$ to K.

Within the optimization approach, the problem will be solved in the least square sense and can be stated as follows.

Given boundary conditions

$$\begin{cases} \dfrac{\partial T}{\partial x} = q_0(y) & at \quad x = 0; \\ c_{11}T + c_{12}\dfrac{\partial T}{\partial y} + c_{13} = 0 & at \quad y = 0; \\ c_{21}T + c_{22}\dfrac{\partial T}{\partial y} + c_{23} = 0 & at \quad y = 1 \end{cases} \tag{4.8}$$

and measured temperature values T_m along the boundary D_m at $x = 0$, find the boundary heat flux q along the boundary D at $x = L$, with

$$q \in L^2[D], \tag{4.9}$$

that minimizes the object functional

$$\begin{aligned} E(q) &= \frac{1}{2} \parallel T(r,q) - T_m(r) \parallel^2_{L^2[D_m]} \\ &= \frac{1}{2}\int_{D_m} (T(r,q) - T_m(r))^2 \, dD_m \\ &= \frac{1}{2}\int_0^1 (T(0,y,q) - T_m(y))^2 \, dy \end{aligned} \tag{4.10}$$

where

$$q = \left.\frac{\partial T}{\partial x}\right|_{x=L} \tag{4.11}$$

and $L^2[D]$ is the square integrable function space that the minimization occurs.

Note that to reduce unnecessary complications of the problem, it is assumed that $H(r)$ is λq according to Eq. 4.5.

4.2 Method of Solution

The inverse problem has been formulated in the form of an optimization problem. The optimization algorithm starts with an initial guess of the unknown function. In this study, the minimization of the object functional Eq. 4.10 consists of constructing by some descent method a sequence of approximation q^0, q^1, ..., q^k, q^{k+1}, ... The conjugate gradient method is adopted here since it converges usually faster than the steepest descent method. It gives iteratively

$$q^{k+1} = q^k + \alpha^k p^k \tag{4.12}$$

where α^k is the step size and p^k the conjugate search direction, which is related to the gradient of E with respect to the function q^k.

4.2.1 The Conjugate Technique

The general strategy of optimization process described above consists of two major steps. First is the determination of the search direction p, and second is the determinations of the step size α which minimizes $E(q)$ in the direction p [61, 45].

The conjugate direction method is a first-order method as well as the steepest descent method. They both use gradient information to determine search directions. The steepest descent method simply takes the negative of the gradient of the objective function as the search direction. That is, at iteration k

$$p^k = -\nabla E(q^k). \tag{4.13}$$

Due to the fact that it does not utilize information from previous iterations in order to accelerate the convergence, the convergence rate of this method is rather poor.

The Polak-Ribiere version [62] of the conjugate direction technique requires only a simple modification to the steepest descent algorithm and yet dramatically improves the convergence rate of the optimization process. It is accomplished by specifying an initial search vector as the steepest descent direction defined by Eq.

4.13. On subsequent iterations a conjugate direction is defined as

$$p^k = -\nabla E(q^k) + \beta^k p^{k-1} \tag{4.14}$$

where the scalar β^k is defined as

$$\beta^k = \frac{\langle (\nabla E^k - \nabla E^{k-1}), \nabla E^k \rangle_{L^2[D]}}{\|\nabla E^{k-1}\|^2_{L^2[D]}}. \tag{4.15}$$

Once a search direction P^k is found, it can be shown that the objective functional E will reach a minimum in that direction if q^k makes a step α^k as indicated in Eq. 4.12 with

$$\alpha = -\frac{< \nabla E, p >_{L^2[D]}}{\|\dot{T}(D_m)\|^2_{L^2[D_m]}}. \tag{4.16}$$

where $\dot{T}$ is the so-called temperature sensitivity as defined below.

Before proceeding further, let us recall that the gradient of $E(q)$, at point q, denoted by $\nabla E(q)$, is related to the directional derivative of E at this point. The directional derivative of E at q in the direction Δq, denoted by $D_{\Delta q}E(q)$, is defined by

$$D_{\Delta q}E(q) = \lim_{\epsilon \to 0} \frac{E(q + \epsilon \Delta q) - E(q)}{\epsilon} \tag{4.17}$$

and it is related to the gradient $\nabla E(q)$ by

$$D_{\Delta q}E(q) = \langle \nabla E(q) \,|\, \Delta q \rangle_{L^2[D]}. \tag{4.18}$$

In the present function space $L^2[D]$,

$$\begin{aligned} D_{\Delta q}E(q) &= \int_D \nabla E(q) \Delta q \, dD \\ &= \int_0^1 \nabla E(q) \Delta q \, dy. \end{aligned} \tag{4.19}$$

Note that the dimensionality for this optimization problem is determined by the dimension of the minimization function space. When a priori information is available, i.e., q can be expressed in terms of a set of basis functions q_i, $(i = 1, 2, ..., N_D)$, the problem is a minimization in a finite N_D-dimensional function space. The gradient $\nabla E(q)$ in this case can be determined in a rather straightforward way by the standard differential calculus. In the present study, we will not require any priori information on the nature of the function to be solved. The optimization problem is then infinite-dimensional. To compute the gradient of $E(q)$, it is necessary to develop an adjoint problem in conjunction with a sensitivity problem as described in the following two sections.

4.2.2 The Sensitivity Problem

Let the temperature sensitivity $\tilde{T}$ be defined as the directional derivative of T at q in the direction Δq, i.e.,

$$\tilde{T}(x, y) = D_{\Delta q} T(x, y : q). \tag{4.20}$$

Based on this definition and Eq. 3.1, the sensitivity problem is straightforward derived as

$$\nabla^2 \tilde{T} = 0 \tag{4.21}$$

with the conditions

$$\begin{cases} \tilde{q}_0 = 0 & at \quad x = 0; \\ \tilde{q} = \Delta q & at \quad x = L; \\ c_{11}\tilde{T} + c_{12}\dfrac{\partial \tilde{T}}{\partial y} = 0 & at \quad y = 0; \\ c_{21}\tilde{T} + c_{22}\dfrac{\partial \tilde{T}}{\partial y} = 0 & at \quad y = 1. \end{cases} \tag{4.22}$$

4.2.3 The Adjoint Problem

For an infinite dimensional space where the minimization occurs, the gradient ∇E may be obtained from the solution of the so-called adjoint problem. The details of the derivation were given by Nguyen [24, 26]. Only brief description is given here.

The adjoint problem is defined as

$$\nabla^2 T^* = 0 \tag{4.23}$$

with the conditions

$$\begin{cases} q_0^* = T_m - T & at \quad x = 0; \\ q^* = 0 & at \quad x = L; \\ c_{11}T^* + c_{12}\dfrac{\partial T^*}{\partial y} = 0 & at \quad y = 0; \\ c_{21}T^* + c_{22}\dfrac{\partial T^*}{\partial y} = 0 & at \quad y = 1. \end{cases} \tag{4.24}$$

The driving force of the adjoint problem is the error between the given temperature measurement T_m and calculated temperature T at $x = 0$.

Recall that the gradient $\nabla E(q)$ is related to its directional derivative by

$$D_{\Delta q}E(q) = \int_D \nabla E(q)\Delta q \, dD. \tag{4.25}$$

While it follows from Eq. 4.10 that

$$D_{\Delta q}E(q) = \int_{D_m} (T - T_m)\tilde{T} \, dD_m. \tag{4.26}$$

From Eq. 4.25 and Eq. 4.26 we readily deduce that

$$\int_D \nabla E(q)\Delta q \, dD = \int_D T^*(D)\Delta q \, dD. \tag{4.27}$$

The gradient of the object functional, $\nabla E(q)$, is therefore equal to the adjoint temperature at the boundary where unknown unknown heat flux q is to be found, i.e.,

$$\nabla E = T^*(D) = T^*(L, y). \tag{4.28}$$

4.2.4 Algorithm of Solution by Conjugate Gradient

The optimization algorithm with conjugate gradient technique can be summarized as follows [27].

1. Choose initial guess q^0 and set iteration counter $k = 0$;

2. Solve the direct problem with q^k to obtain T^k and calculate the current value of

$$\begin{aligned} E(q^k) &= \frac{1}{2} \parallel T(r:q) - T_m(r) \parallel^2_{L^2[D_m]} \\ &= \frac{1}{2} \int_0^1 (T^k(0,y) - T_m(y))^2 \, dy; \end{aligned} \tag{4.29}$$

3. Evaluate the error $T^k - T_m$ on the boundary D_m;

4. Evaluate the gradient $\nabla E^k = T^{*k}(L, y)$ by solving the adjoint problem to obtain T^{*k};

5. Calculate the search direction p^k by

$$p^k = \begin{cases} -\nabla E^k, & if \quad k = 0 \\ -\nabla E(q^k) + \beta^k p^{k-1}, & if \quad k > 0 \end{cases} \tag{4.30}$$

where

$$\beta^k = \frac{< \nabla E^k - \nabla E^{k-1}, \nabla E^k >_{L^2[D]}}{\| \nabla E^{k-1} \|^2_{L^2[D]}}; \tag{4.31}$$

6. Calculate the step size

$$\alpha = -\frac{< \nabla E, p >_{L^2[D]}}{\|\tilde{T}(D_m)\|^2_{L^2[D_m]}} \tag{4.32}$$

by solving the sensitivity problem with $\Delta q = p^k$ to obtain $\tilde{T}^k$;

7. Update

$$q^{k+1} = q^k + \alpha^k p^k; \tag{4.33}$$

8. Set $k = k + 1$, go back to step 2, repeat until convergence criterion $E(q^k) < \epsilon$ or $k > k_{max}$ is satisfied.

The above algorithm actually involves the solutions of three diffusion equations, namely the direct, sensitivity and adjoint equations at every step of the sequence of approximations for the minimizer. As described in the following sections, these equations are of the same type and may be solved by any appropriate method.

In the present study, the control volume approach is used to obtain the discretized equations which are then solved by the line-by-line method.

4.3 Solution Analysis: Exact Data

4.3.1 Study of Truncation Error

The case to be tested is

$$\begin{cases} T_m = -\dfrac{\epsilon sin(n\pi y)}{n\pi sinh(n\pi L)} & at \quad x = 0; \\ q_0 = 0 & at \quad x = 0; \\ T = 0 & at \quad y = 0; \\ T = 0 & at \quad y = 1; \\ S(x,y) = 0 \end{cases} \tag{4.34}$$

where ϵ and n are constant coefficients.

Let us note that the exact solution satisfying the above data can be found as

$$T = -\frac{\epsilon cosh(n\pi x) sin(n\pi y)}{n\pi sinh(n\pi L)}. \tag{4.35}$$

Hence, the expected result of q is

$$q = -\epsilon sin(n\pi y) \qquad at \qquad x = L. \tag{4.36}$$

Cases with different combinations of coefficients n and ϵ are tested in the domain $L = 1$ to show that truncation error plays an important role in the performance of the optimization. This is because that we are dealing here with very stiff functions. It gets more significant when n increases. Fig. 4.1 shows the temperature values near the boundary $x = 0$ are very small, resulting in the loss of significant figures during the computation.

One can measure the performance of the method by checking how precise q can be optimized to its exact value, i.e., Eq. 4.36.

For $\epsilon = 1$, $n = 1$, the solution with a 21×21 mesh is good as q matches the exact curve very well (Fig. 4.2). However, when $n = 2$, q converges to about 0 (Fig. 4.3)! Increasing the mesh size doesn't do any good because it can only improve the precision of the discretization but not the significant decimal figures of the machine's floating point operation. The optimization process thus fails to converge towards the expected value due to the effects of truncation errors.

To understand these effects, it is necessary to trace the calculations step by step to find out at which step of the algorithm the main error occurs. In fact, mathematically, the method is supposed to give the exact solution after just one iteration. It is demonstrated below.

According to the algorithm, let $k = 0$ and q is guessed to be 0. The first iteration then consists of solving the direct problem with the following boundary conditions:

$$\begin{cases} q_0 = 0 & at \quad x = 0; \\ q = 0 & at \quad x = 1; \\ T = 0 & at \quad y = 0; \\ T = 0 & at \quad y = 1; \\ S(x, y) = 0. \end{cases} \tag{4.37}$$

The solution is

$$T = 0. \tag{4.38}$$

Then comes the adjoint problem to determine ∇E. The boundary conditions

are

$$\begin{cases} q_0^* = T_m - T = T_m = -\dfrac{\epsilon sin(n\pi y)}{n\pi sinh(n\pi L)} & at \quad x = 0; \\ q^* = 0 & at \quad x = 1; \\ T^* = 0 & at \quad y = 0; \\ T^* = 0 & at \quad y = 1; \\ S^*(x,y) = 0. \end{cases} \tag{4.39}$$

The solution is

$$T^* = \frac{\epsilon cosh(n\pi(x-L))sin(n\pi y)}{(n\pi sinh(n\pi L))^2} \tag{4.40}$$

and

$$\frac{\partial T^*}{\partial x} = \frac{\epsilon sinh(n\pi(x-L))sin(n\pi y)}{n\pi sinh^2(n\pi L)}. \tag{4.41}$$

We thus obtain

$$\nabla E = T^*\Big|_{x=L} = \frac{\epsilon sin(n\pi y)}{(n\pi sinhhn\pi L)^2}. \tag{4.42}$$

The step size is determined by the sensitivity $\tilde{T}$ which results from the sensitivity problem

$$\begin{cases} \tilde{q}_0 = 0 & at \quad x = 0; \\ \tilde{q} = p = -\nabla E = -\dfrac{\epsilon sin(n\pi y)}{(n\pi sinh(n\pi L))^2} & at \quad x = 1; \\ \tilde{T} = 0 & at \quad y = 0; \\ \tilde{T} = 0 & at \quad y = 1; \\ \tilde{S}(x,y) = 0. \end{cases} \tag{4.43}$$

The solution is

$$\tilde{T} = \frac{\epsilon cosh(n\pi x) sin(n\pi y)}{(n\pi sinh(n\pi L))^3} \tag{4.44}$$

and the step size is

$$\begin{aligned}
\alpha &= -\frac{< \nabla E, p >_{L^2[D]}}{\|\tilde{T}(D_m)\|^2_{L^2[D_m]}} \\
&= -\frac{< \nabla E, \nabla E >_{L^2[D]}}{\|\tilde{T}(D_m)\|^2_{L^2[D_m]}} \\
&= -\frac{\|\nabla E\|^2_{L^2[D]}}{\|\tilde{T}(0,y)\|^2_{L^2[D_m]}} \\
&= -\frac{\left\| \frac{\epsilon sin(n\pi y)}{(n\pi sinh(n\pi L))^2} \right\|^2_{L^2[y\in[0,1]]}}{\left\| \frac{\epsilon sin(n\pi y)}{(n\pi sinh(n\pi L))^3} \right\|^2_{L^2[y\in[0,1]]}} \\
&= (n\pi sinh(n\pi L))^2.
\end{aligned} \tag{4.45}$$

The updated value for q is therefore

$$\begin{aligned}
q^1 &= q^0 + \alpha p \\
&= (n\pi sinh(n\pi L))^2 \cdot (-\frac{\epsilon sin(n\pi y)}{(n\pi sinh(n\pi L))^2}) \\
&= -\epsilon sin(n\pi y).
\end{aligned} \tag{4.46}$$

which is the expected (exact) value as shown in Eq. 4.36.

Based on the above exact solutions at each step of the first iteration, one can check the numerical results as shown in Table. 4.1 for the case $\epsilon = 1$, $n = 2$. From this table it appears that the main error occurs in the computation of $\tilde{T}$. Up to ∇E, the numerical results have relatively small error compared with the exact analytical results. However, the solution of $\tilde{T}(0, y)$ is about 100 times larger than exact solution. It leads to a very small optimization step $\alpha = 168.182$ while the exact

value is 2.83e+06. Although the optimization direction (∇E at the first iteration) is right, q remains therefore very close to the initial value 0.

Note that the main error happens in the solution of $\tilde{T}$ because the exact solution

$$\tilde{T} = \frac{cosh(2\pi x)sin(2\pi y)}{(2\pi sinh(2\pi L))^3}, \tag{4.47}$$

with a magnitude of around 10^{-12} to 10^{-14}, is actually too small for the program to solve. The machine's floating point operation is not precise enough in the case.

For the case $\epsilon = 1$, $n = 1$ which has a perfect result (Fig. 4.2), the solution of q after the first iteration is not what it's supposed to be. Table. 4.2 shows that the sensitivity problem of this case also has about 10% error and q differs from the exact solution pretty much (see also Fig. 4.4). However, after several iterations q converges to the exact solution. The explanation is that the truncation error makes some trouble in the sensitivity problem but not as much as that in the last case. The optimization program can still make q converge after several iterations instead of staying at the initial value as in the last case.

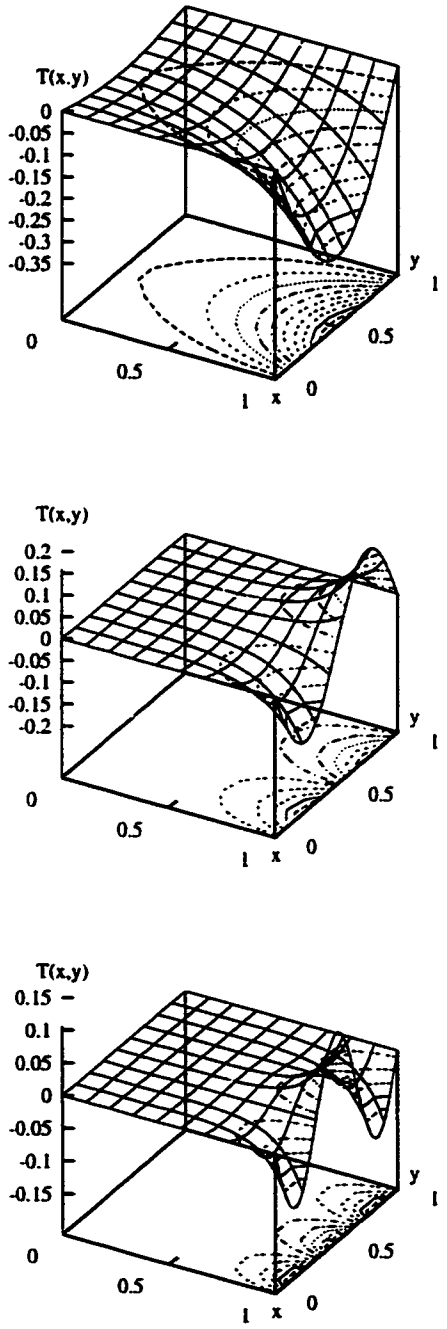

Figure 4.1: Exact solutions of $T = -\frac{\epsilon cosh(n\pi x)sin(n\pi y)}{n\pi sinh(n\pi L)}$, $\epsilon = 1$, (1) $n = 1$; (2) $n = 2$; (3) $n = 3$

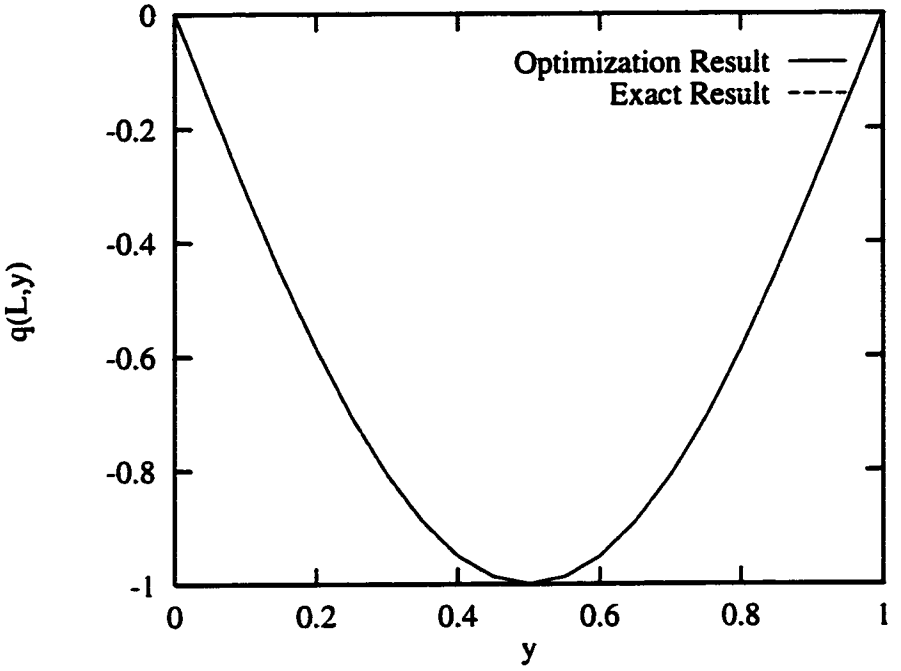

Figure 4.2: Result of q for $T = -\frac{\epsilon cosh(n\pi x)sin(n\pi y)}{n\pi sinh(n\pi L)}$, $\epsilon = 1$, $n = 1$, after 11 itrs.

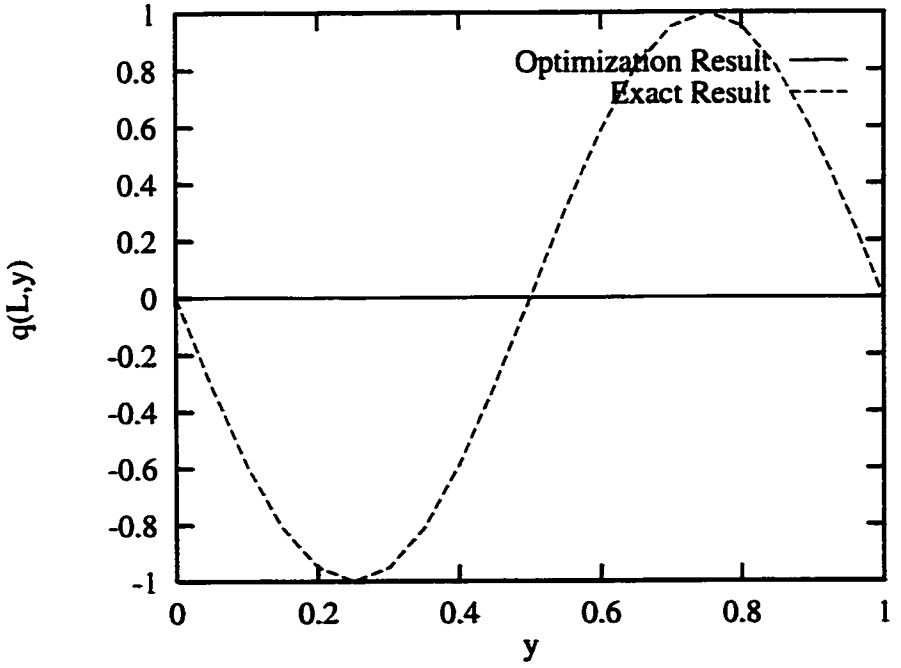

Figure 4.3: Result of q for $T = -\frac{\epsilon cosh(n\pi x)sin(n\pi y)}{n\pi sinh(n\pi L)}$, $\epsilon = 1$, $n = 2$, after 9 itrs.

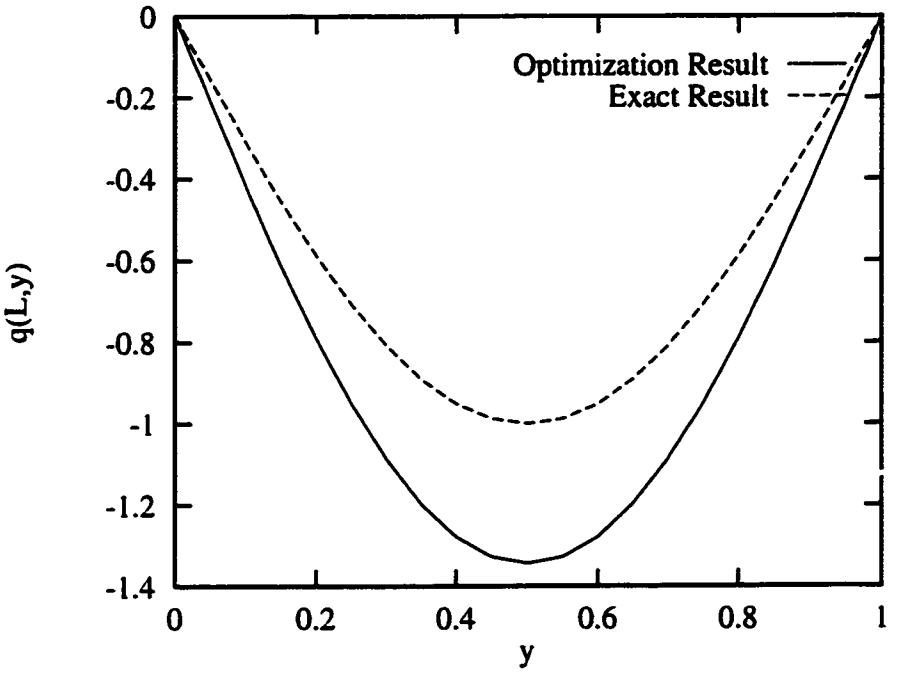

Figure 4.4: Result of q after the first iteration for $T = -\frac{\epsilon cosh(n\pi x)sin(n\pi y)}{n\pi sinh(n\pi L)}$, $\epsilon = 1$, $n = 1$

4.3.2 Two Ways to Avoid Truncation Error

There are two ways to deal with truncation error. One is to renormalize the solution to make it larger than the real solution. More specifically, if a case with solution $T(x, y)$ is too small to solve, it's possible to firstly look for $cT(x, y)$, where c is a constant larger than 1, by making appropriate modification to the given boundary conditions. This technique is suitable for the present case.

As shown by Fig. 4.3, the optimization algorithm to find the solution

$$T = -\frac{cosh(2\pi x)sin(2\pi y)}{2\pi sinh(2\pi L)} \tag{4.48}$$

y	∇E	$(\nabla E)_e$	$\tilde{T}(0,y)$	$(\tilde{T}(0,y))_e$	q	$(q)_e$
0.0	0	0	0	-0	0	0
0.1	2.25526e-07	2.0769e-07	9.23723e-09	-1.23457e-10	-3.79295e-05	-0.587785
0.2	3.67205e-07	3.3605e-07	1.73255e-08	-1.99758e-10	-6.17572e-05	-0.951057
0.3	3.73119e-07	3.3605e-07	2.35689e-08	-1.99758e-10	-6.27519e-05	-0.951057
0.4	2.42732e-07	2.0769e-07	2.74215e-08	-1.23457e-10	-4.08231e-05	-0.587785
0.5	2.69292e-08	4.32722e-23	2.85551e-08	-2.57222e-26	-4.52901e-06	-1.22465e-16
0.6	-1.91508e-07	-2.0769e-07	2.68964e-08	1.23457e-10	3.22082e-05	0.587785
0.7	-3.29544e-07	-3.3605e-07	2.26433e-08	1.99758e-10	5.54233e-05	0.951057
0.8	-3.35547e-07	-3.3605e-07	1.62541e-08	1.99758e-10	5.64329e-05	0.951057
0.9	-2.08895e-07	-2.0769e-07	8.40869e-09	1.23457e-10	3.51323e-05	0.587785
1.0	0	-8.65443e-23	0	5.14443e-26	0	0.44929e-16

Table 4.1: Comparison of the numerical and exact solutions of the first iteration for the case $\epsilon = 1$, $n = 2$

y	∇E	$(\nabla E)_e$	$\tilde{T}(0,y)$	$(\tilde{T}(0,y))_e$	q	$(q)_e$
0.0	0	0	0	-0	0	-0
0.1	0.0002367	0.000234754	-5.59411e-06	-6.47037e-06	-0.415485	-0.309017
0.2	0.000450212	0.000446529	-1.06689e-05	-1.23074e-05	-0.790268	-0.587785
0.3	0.000619639	0.000614595	-1.47203e-05	-1.69396e-05	-1.08767	-0.809017
0.4	0.000728399	0.000722499	-1.73453e-05	-1.99137e-05	-1.27858	-0.951057
0.5	0.000765852	0.000759681	-1.82797e-05	-2.09386e-05	-1.34432	-1
0.6	0.000728339	0.000722499	-1.74245e-05	-1.99137e-05	-1.27847	-0.951057
0.7	0.000619537	0.000614595	-1.4856e-05	-1.69396e-05	-1.08749	-0.809017
0.8	0.000450101	0.000446529	-1.08192e-05	-1.23074e-05	-0.790073	-0.587785
0.9	0.000236621	0.000234754	-5.70359e-06	-6.47037e-06	-0.415347	-0.309017
1.0	0	9.30341e-20	0	-2.56423e-21	0	-1.22465e-16

Table 4.2: Comparison of the numerical and exact solutions of the first iteration for the case $\epsilon = 1$, $n = 1$

was unsuccessful because of truncation errors. However, if the given boundary conditions are changed to

$$\begin{cases} T_m = -\dfrac{1000sin(2\pi y)}{2\pi sinh(2\pi L)} & at \quad x = 0; \\ q_0 = 0 & at \quad x = 0; \\ T = 0 & at \quad y = 0; \\ T = 0 & at \quad y = 1; \\ S(x,y) = 0, \end{cases} \tag{4.49}$$

the new solution will be

$$T = -\frac{1000cosh(2\pi x)sin(2\pi y)}{2\pi sinh(2\pi L)}. \tag{4.50}$$

If this new solution can be obtained correctly, the real solution is straight forward.

Actually, for the modified case the method comes up with a nice solution. Fig. 4.5 is the optimization result of q_1 of the modified case after 11 iterations. Fig. 4.6 is the final solution of the original case. It looks quite similar to its exact solution Fig. 4.1-(2). In fact, the error is less than 2%.

Now comes the question of how large at least should the original problem be amplified, i.e., the determination of c. From the above analysis, it appears that the main error occurs in the calculation of the sensitivity. Then the key point of the amplification technique is to increase the magnitude of the sensitivity problem. This is not to say that the sensitivity problem has to be solved exactly to get exact q after just 1 iteration as in mathematical formulation. It is enough as long as q converges to the exact result even after several iterations.

Take the last case for example. Although the original case

$$T = -\frac{cosh(2\pi x)sin(2\pi y)}{2\pi sinh(2\pi L)} \tag{4.51}$$

was amplified 1000 times to

$$T = -\frac{1000cosh(2\pi x)sin(2\pi y)}{2\pi sinh(2\pi L)}, \tag{4.52}$$

the sensitivity of the first iteration still has huge error (10 times larger than exact value, see Table. 4.3). However, q made a small step toward the exact solution instead of staying at 0. After 11 iterations q reached the exact solution well. Fig. 4.7 and Fig. 4.8 show the optimization process clearly.

Renormalization technique is applicable to the linear partial differential function as in the present study. For linear equation it is possible to modify the boundary conditions according to the scale c and solve the same equation with the new boundary conditions. For nonlinear equation not only the boundary conditions have to be changed but also the equation itself, resulting in a much more complicate numerical implementation.

Another way to avoid the influence of truncation error is simpler. For a certain temperature field which can't be predicted accurately from the measurements, one can try to move the sensors closer to the unknown boundary.

For the present case

$$T = -\frac{\epsilon cosh(n\pi x)sin(n\pi y)}{n\pi sinh(n\pi L)} \tag{4.53}$$

which has trouble to solve when $n \gg 1$, some numerical experiments are done by making measurements closer to $x = L$. Successful results are obtained. The higher the n is, the closer the measurements have to be. Fig. 4.9 shows the three cases of $\epsilon = 1$, $n = 2$, 3, and 4. The domains are $x \in [0.25, 1]$, $x \in [0.55, 1]$ and $x \in [0.7, 1]$, respectively.

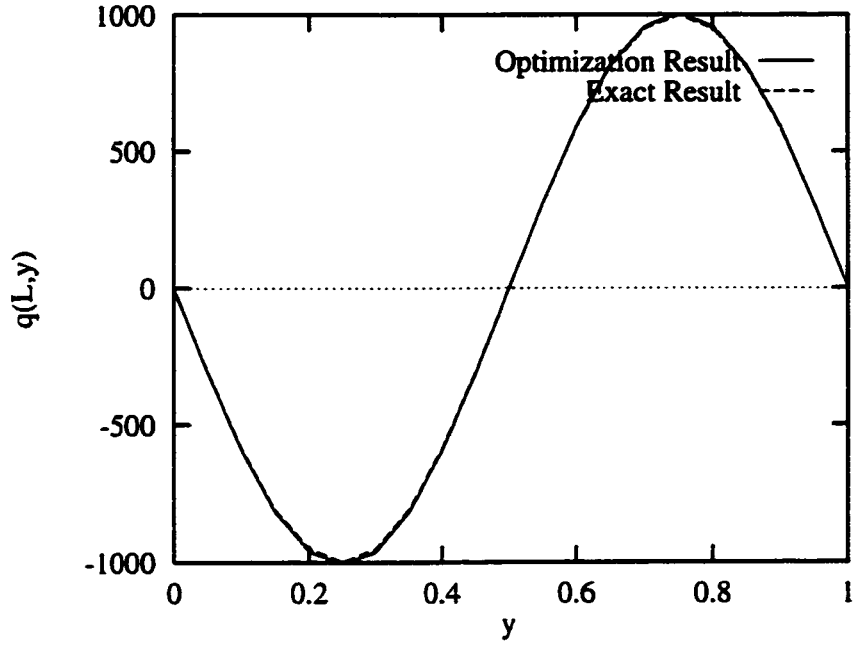

Figure 4.5: Result of q for the modified case $T = -\frac{1000cosh(2\pi x)sin(2\pi y)}{2\pi sinh(2\pi L)}$, after 11 itrs.

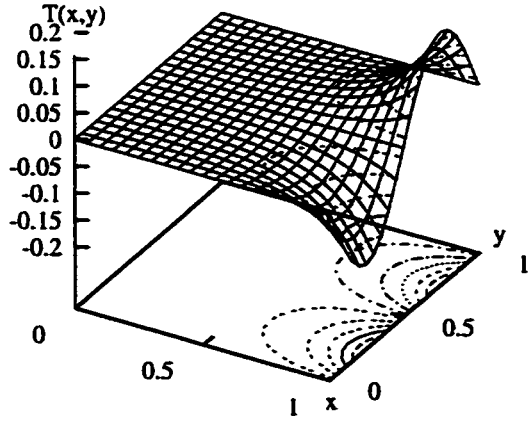

Figure 4.6: Final solution of $T = -\frac{cosh(2\pi x)sin(2\pi y)}{2\pi sinh(2\pi L)}$

y	∇E	$(\nabla E)_e$	$\tilde{T}(0,y)$	$(\tilde{T}(0,y))_e$	q	$(q)_e$
0.0	0	0	0	-0	0	-0
0.1	0.000217701	0.00020769	8.00039e-07	-1.23457e-07	-3.64347	-587.785
0.2	0.000352478	0.00033605	1.53177e-06	-1.99758e-07	-5.8991	-951.057
0.3	0.000353068	0.00033605	2.15439e-06	-1.99758e-07	-5.90898	-951.057
0.4	0.00021942	0.00020769	2.61347e-06	-1.23457e-07	-3.67224	-587.785
0.5	2.69009e-06	4.32722e-20	2.84766e-06	-2.57222e-23	0.0450216	-1.22465e-13
0.6	-0.000214303	-0.00020769	2.80339e-06	1.23457e-07	3.5866	587.785
0.7	-0.000348716	-0.00033605	2.45412e-06	1.99758e-07	5.83613	951.057
0.8	-0.000349315	-0.00033605	1.81695e-06	1.99758e-07	5.84617	951.057
0.9	-0.00021604	-0.00020769	9.597e-07	1.23457e-07	3.61566	587.785
1.0	0	-8.65443e-20	0	5.14443e-23	0	2.44929e-13

Table 4.3: Comparison of the numerical and exact solutions of the first iteration for the case $\epsilon = 1000$, $n = 2$

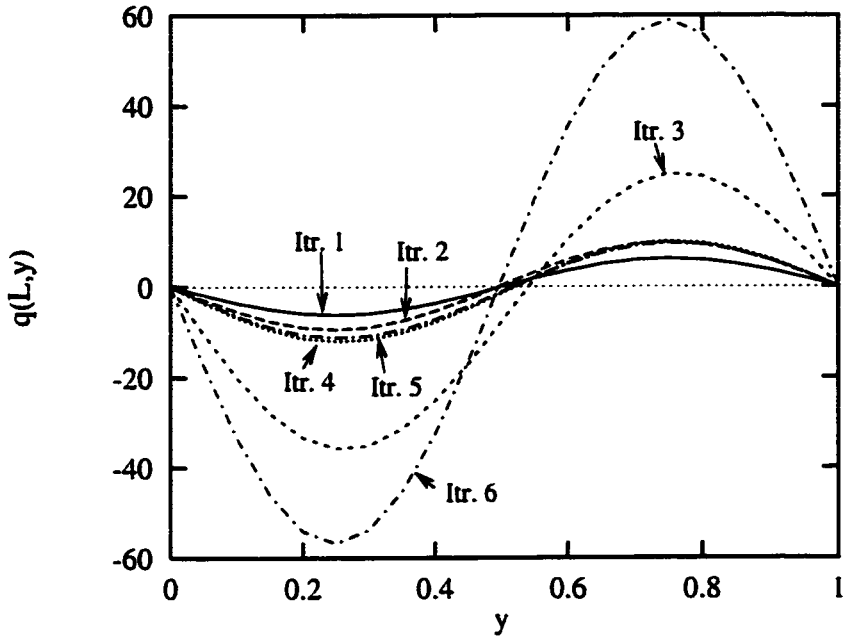

Figure 4.7: Optimization process of $T = -\frac{1000cosh(2\pi x)sin(2\pi y)}{2\pi sinh(2\pi L)}$, (Itr. 1-6)

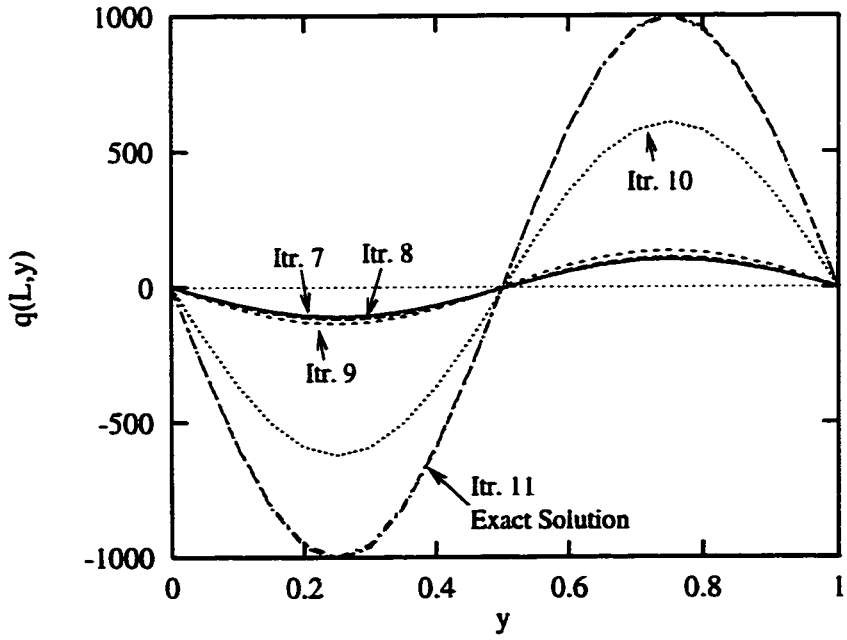

Figure 4.8: Optimization process of $T = -\frac{1000cosh(2\pi x)sin(2\pi y)}{2\pi sinh(2\pi L)}$, (Itr. 7-11)

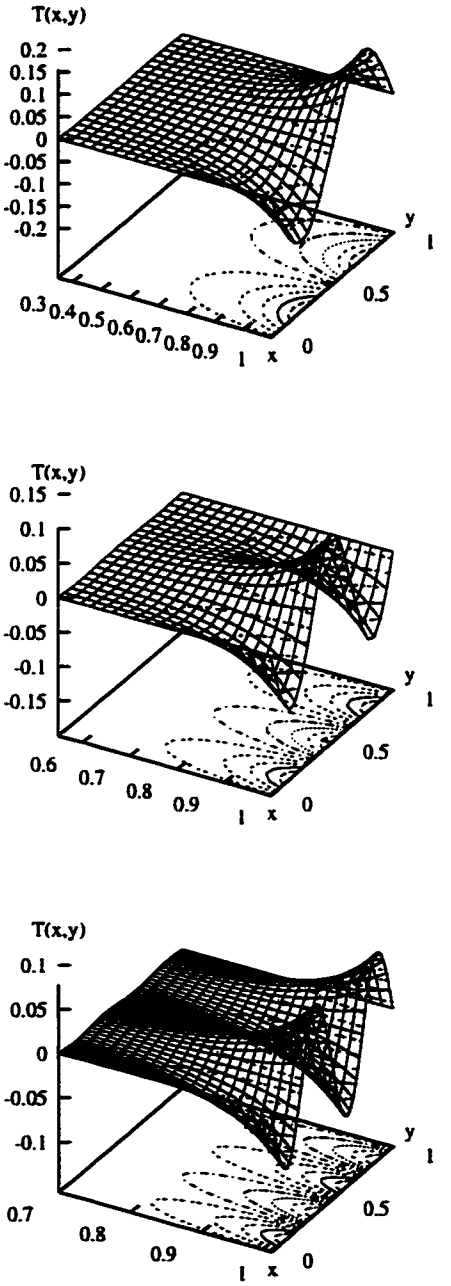

Figure 4.9: Solutions of $T = -\frac{\epsilon cosh(n\pi x)sin(n\pi y)}{n\pi sinh(n\pi L)}$, $\epsilon = 1$ after 10 itrs. by moving the sensors forward (1) $n = 2$; (2) $n = 3$; (3) $n = 4$

4.3.3 Multi-Frequency Boundary Heat Flux q

The cases studied before are limited in that the predicted boundary heat flux q consists of a single frequency. The analysis of more complicate cases will be based on the conclusions drawn previously from the single frequency cases because a function can be decomposed to a Fourier series as long as it satisfies the Dirichlet conditions, i.e., it has only a finite number of finite discontinuities and only a finite number of extreme values. Functions satisfying these conditions may be called piecewise regular. In the vast majority of physical problems involving a Fourier series these conditions are satisfied.

Take an example of boundary heat flux at $x = 1$

$$q = 1 - 2|y - 0.5| \tag{4.54}$$

and

$$\begin{cases} q_0 = 0 & at \quad x = 0; \\ T = 0 & at \quad y = 0; \\ T = 0 & at \quad y = 1; \\ S(x, y) = 0. \end{cases} \tag{4.55}$$

The temperature distribution in this case can be calculated by solving a direct problem under the above conditions. Then an inverse problem based on these simulated data can be set up to test how the optimization method can recover the heat flux q by proceeding as follows.

Once $T(x, y)$ has been solved under the above boundary conditions, the heat flux at any point between $x = 0$ and $x = 1$ can be obtained by central difference:

$$q_{i,j} = \frac{q_{i+1,j} - q_{i-1,j}}{2\Delta x}. \tag{4.56}$$

The simulated data for the inverse problem are then

$$\begin{cases} q_0 = q(x_o, y) & at \quad x = x_o; \\ T = T(x_o, y) & at \quad x = x_o; \\ T = 0 & at \quad y = 0; \\ T = 0 & at \quad y = 1; \\ S(x, y) = 0 \end{cases} \tag{4.57}$$

where x_o is the site where the sensors are located.

Fig. 4.10 includes the optimization results of q with $x_o = 0$, 0.25, 0.5, 0.75 and 0.9. One can find that the results with $x_o = 0$, 0.25 and 0.5 are about the same. This can be explained from the previous study of truncation error.

It is obvious that q satisfies the Dirichlet conditions. It can be represented by a Fourier series.

$$q = \frac{8}{\pi^2} \sum_{n=1}^{\infty} (-1)^{n-1} \frac{sin(2n-1)\pi y}{(2n-1)^2}$$

$$= \frac{8}{\pi^2}(sin(\pi y) - \frac{1}{3^2} sin(3\pi y) + \frac{1}{5^2} sin(5\pi y) - ...) \tag{4.58}$$

Now that $T = 0$ at $y = 0$ and $y = 1$, the solution can be decomposed to a series whose terms are respectively the solutions corresponding to the Fourier series term of q as the heat flux at $x = 1$.

As stated in the last section, if q has relatively high frequency the truncation error will increase significantly. To avoid the truncation error the sensors have to be moved closer to the predicted boundary. Fig. 4.11, Fig. 4.12 and Fig. 4.13 are the results with the first three terms of q as the boundary heat flux at $x = 1$. It is found that to get correct solutions the sensors have to be put at $x_o = 0$, $x_o = 0.75$

and $x_o = 0.9$, respectively. The results of q with $x_o = 0$, 0.25 and 0.5 are the same because under these three circumstances only the first term of q is solved correctly. It can be demonstrated by comparing the curves of $x_o = 0$, 0.25 and 0.5 in Fig. 4.10 with the Fig. 4.11, the result of the first term. They are about the same.

While $x_o = 0.75$ and $x_o = 0.9$ the second and the third terms can be obtained right. As the result, the solution of q gets closer to the exact solution (Fig. 4.10).

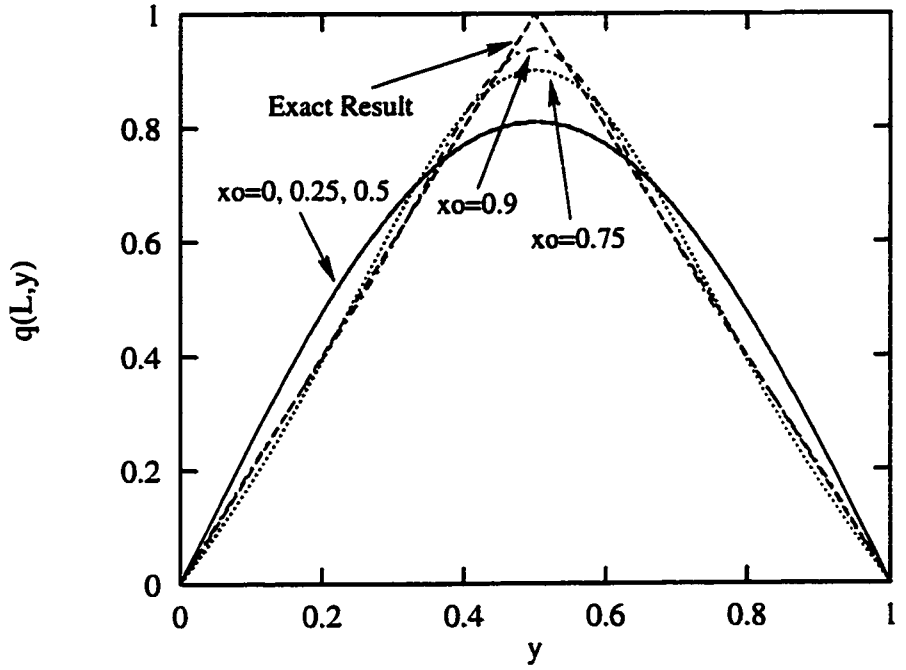

Figure 4.10: Optimization results of q aT different x_o

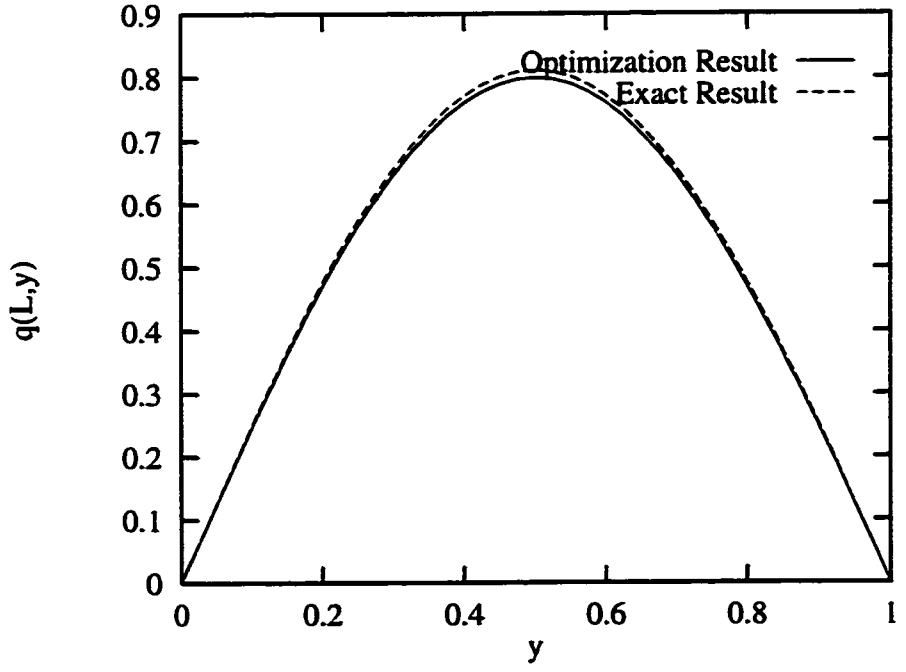

Figure 4.11: Optimization result ($x_o = 0$) of the first term $\frac{8}{\pi^2} sin(\pi y)$

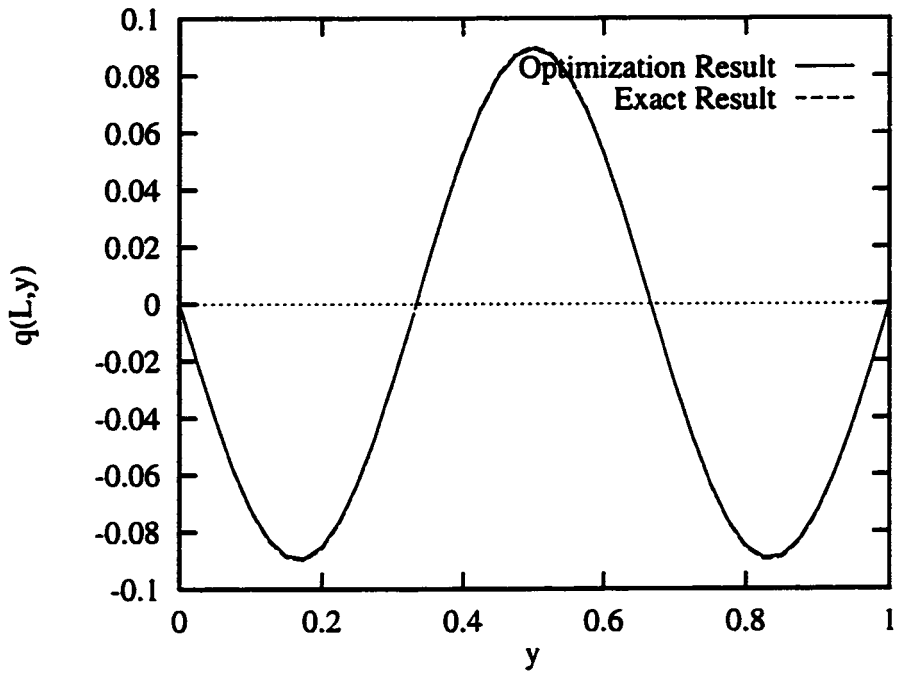

Figure 4.12: Optimization result ($x_o = 0.75$) of the second term $-\frac{8}{9\pi^2}sin(3\pi y)$

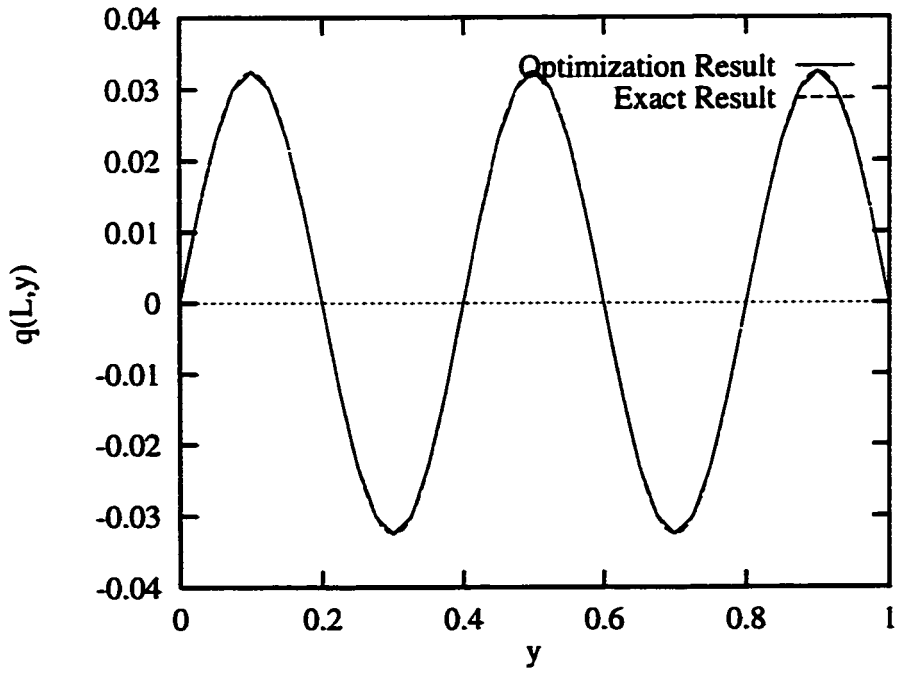

Figure 4.13: Optimization result ($x_o = 0.9$) of the third term $\frac{8}{25\pi^2}sin(5\pi y)$

4.4 Study of Random Error: Noisy Data

The previous tests are based on the assumption that the measurement of the boundary conditions are exact. This is impossible in practice. It is necessary to study the behavior of random error in this method.

Suppose the main error occurs at the measuring of T_m. As the problem is linear, it is convenient to let only a random noise function as T_m to observe its effect. The problem is then

$$\begin{cases} T_m(y) = R(y) = 0.01rand & at \quad x = x_o; \\ q_0 = 0 & at \quad x = x_o; \\ T = 0 & at \quad y = 0; \\ T = 0 & at \quad y = 1. \end{cases} \tag{4.59}$$

Fig. 4.14 includes the results of q obtained with random noise $R(y)$ at different $x_o = 0$, 0.25, 0.5, 0.75 and 0.9. The results give some information about the nature of random noise.

The random noise measured at different x_o lead to errors of predicted heat flux q with different amplitude and frequency. The frequency that can be recovered gets higher when the measured boundary gets closer to the predicted boundary. The amplitude doesn't vary with x_o linearly.

The resolution of a known function into components of different frequencies by means of a Fourier transform is so useful in the last section that in the study of random error one may firstly seek the Fourier series representation of random noise signal. In fact, a random noise function $R(y)$ within the domain $(0, H)$ can be

written in a sine-cosine Fourier series

$$R(y) = R_{c0} + \sum_{n=1}^{\infty} (R_{cn} cos\, n\omega_0 y + R_{sn} sin\, n\omega_0 y) \tag{4.60}$$

where

$$R_{cn} = \frac{2}{H} \int_0^H R(y) cos\, n\omega_0 y\, dy \tag{4.61}$$

and

$$R_{sn} = \frac{2}{H} \int_0^H R(y) sin\, n\omega_0 y\, dy. \tag{4.62}$$

To uncover the properties of random error, one can study the properties of its Fourier series components, just by testing separately its components. The testing cases will be

$$\begin{cases} T_m(y) = \epsilon\, sin\, n\pi y & at \quad x = x_o; \\ q_0 = 0 & at \quad x = x_o; \\ T = 0 & at \quad y = 0; \\ T = 0 & at \quad y = 1. \end{cases} \tag{4.63}$$

The analytical solution is

$$T = \epsilon\, cosh(n\pi(x - x_o)) sin(n\pi y). \tag{4.64}$$

This is also a stiff function as Eq. 4.35. The truncation error may affect the numerical result greatly.

A series of sine function $0.005 sin\, n\pi y$ with n = 1, 2, 3 and 4 are tested at x_o = 0, 0.25 and 0.5. Fig. 4.15 lists the results. The last line of the table in Fig. 4.15 is the cases of

$$T_m = 0.005 \sum_{n=1}^{4} sin(n\pi y) \tag{4.65}$$

at $x_o = 0$, 0.25 and 0.5.

It is not surprising that for certain x_o, the method gets $q(1, y) = 0$ when the frequency of T_m is relatively high. This is all because of the truncation error as studied previously. For $x_o = 0$, cases of $T_m = sin(\pi y)$ and $T_m = sin(2\pi y)$ can be solved right. For $x_o = 0.25$, result of $T_m = sin(3\pi y)$ is good and for $x_o = 0.5$ the method works up to $n = 4$.

It can be concluded that because of truncation error, there is a limit of frequency of error for certain x_o. Error that has higher frequency than this limit does not have effect on the optimized heat flux $q(1, y)$. As a result, the random errors measured at some x_o only affect the solution by its low frequency components. Even though it has a complicate Fourier series representation, one can still see the proof from Fig. 4.14. That is, as x_o approaches the predicted boundary, more and more components of the random error are reflected in the solution of $q(1, y)$, i.e., there are more and more high frequency parts in $q(1, y)$.

This can be understood in the sense that the high frequency parts of random error get lost on the "way" from the measured boundary to the predicted boundary. The longer the "way" is, the more are lost.

The magnitude of error of $q(1, y)$ due to error of $T_m(y)$ is hard to predict. It depends on the random distribution of error. If error at $T_m(y)$ is relatively small compared to its exact value, the optimization result will be still acceptable.

Note that, even at $x_o = 0.9$, the heat flux recovered the first iteration does not contain any information from high frequency components of the random noises.

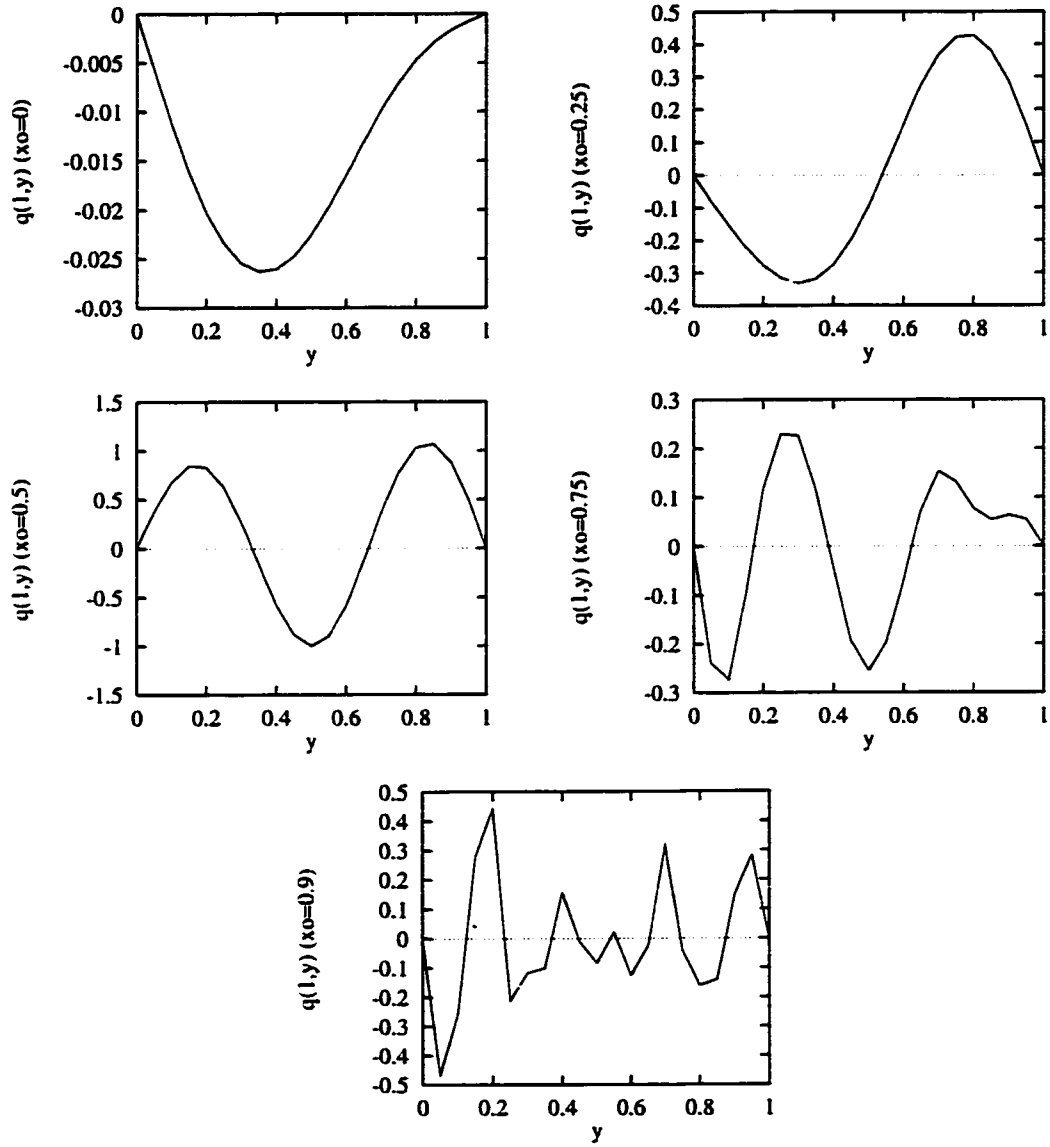

Figure 4.14: Results of q obtained from random noise $R(y)$ at different x_o (0, 0.25, 0.5, 0.75 and 0.9)

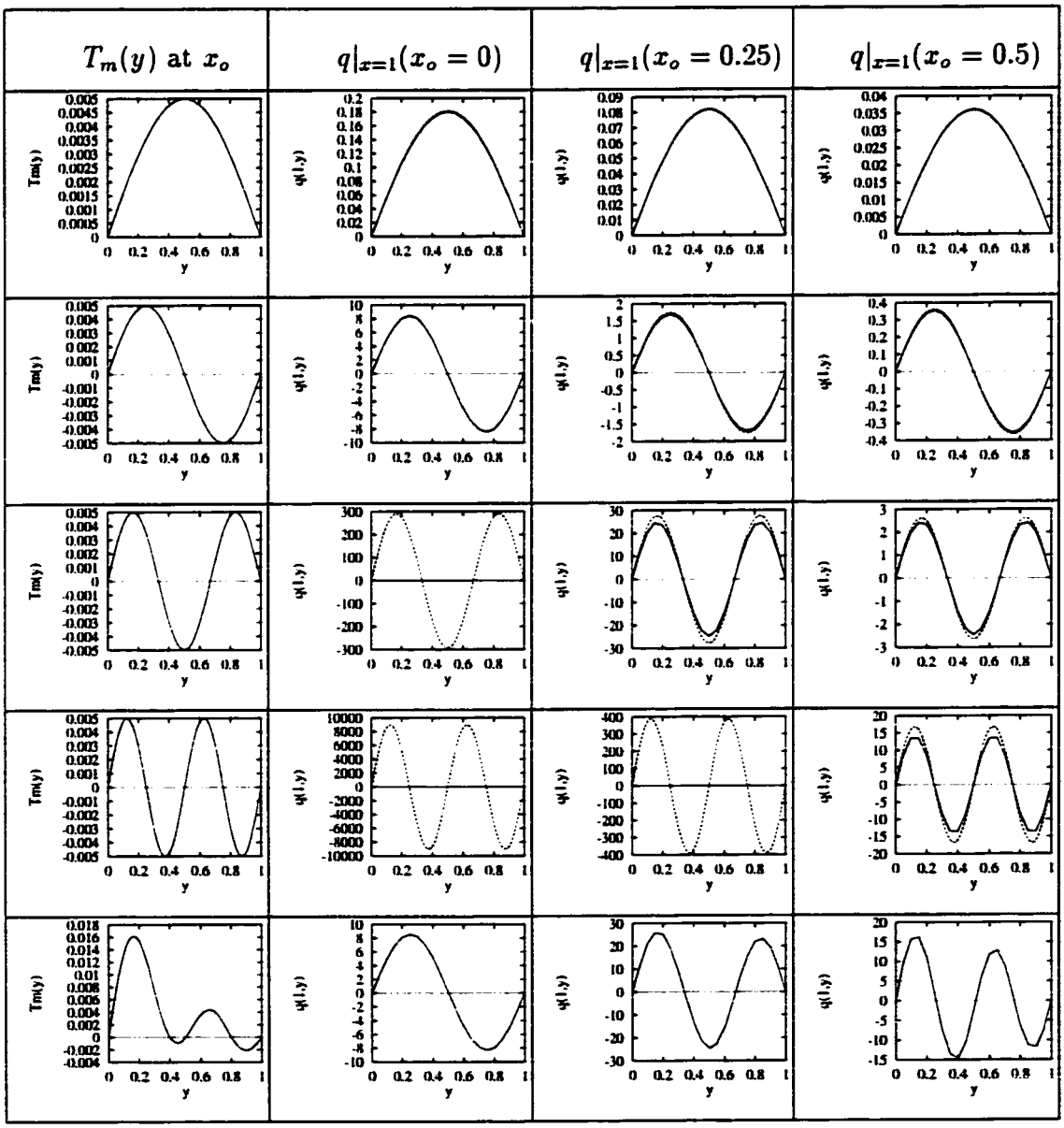

Figure 4.15: Table of $q|_{x=1}$ obtained from $sin\, n\pi y$ at different x_o

CHAPTER V

TIME-DEPENDENT CONDUCTION PROBLEM

This chapter extends the optimization problem of the last chapter to time-dependent problems. The optimization strategy remains the same while some definitions and procedures of the algorithm have to be modified for the unsteady case. The effects errors (both spatial and temporal) are studied as in the last chapter to show that the conjugate gradient can be used in conjunction with the mollification of noisy data to obtain a regularized solution with acceptable accuracy and stability.

5.1 Problem Formulation

The objective of the problem is to solve the time-dependent heat conduction equation

$$\nabla^2 T + S = \frac{\partial T}{\partial t} \tag{5.1}$$

with the conditions

$$\begin{cases} T = T_m(y,t) & at \quad x = L; \\ \dfrac{\partial T}{\partial x} = G_0(y,t) & at \quad x = L; \\ c_{11}T + c_{12}\dfrac{\partial T}{\partial y} + c_{13} = 0 & at \quad y = 0; \\ c_{21}T + c_{22}\dfrac{\partial T}{\partial y} + c_{23} = 0 & at \quad y = 1; \\ T = T_0(x,y) & at \quad t = 0 \end{cases} \tag{5.2}$$

where T_m and G_0 are given functions of y and t.

From the optimization point of view, the problem can be described as follows.

Given conditions

$$\begin{cases} T = T_m(y,t) & at \quad x = L; \\ \dfrac{\partial T}{\partial x} = G_0(y,t) & at \quad x = L; \\ c_{11}T + c_{12}\dfrac{\partial T}{\partial y} + c_{13} = 0 & at \quad y = 0; \\ c_{21}T + c_{22}\dfrac{\partial T}{\partial y} + c_{23} = 0 & at \quad y = 1; \\ T = T_0(x,y) & at \quad t = 0; \end{cases} \tag{5.3}$$

find the boundary heat flux

$$q \in L^2[D,[0,t_f]], \tag{5.4}$$

that minimizes the object functional

$$\begin{aligned} E(q) &= \frac{1}{2} \parallel T(r,t:q) - T_m(r,t) \parallel^2_{L^2[D_m,[0,t_f]]} \\ &= \frac{1}{2}\int_0^{t_f}\int_{D_m} (T(r,t:q) - T_m(r,t))^2 \, dD_m \, dt \\ &= \frac{1}{2}\int_0^{t_f}\int_0^1 (T(L,y,t:q) - T_m(y,t))^2 \, dy \, dt \end{aligned} \tag{5.5}$$

where

$$q = \left.\frac{\partial T}{\partial x}\right|_{x=0}, \tag{5.6}$$

D is the unknown boundary at $x = 0$, and D_m is the measured boundary at $x = L$. $L^2[D, [0, t_f]]$ is the function space that the minimization occurs.

5.2 Method of Solution

The optimization method for time-dependent problem is similar to that for steady problem except some modifications for the nature of time dependence [24].

As in the steady problem, to achieve the minimization of the object functional Eq. 5.5, a sequence of approximation q^0, q^1, ..., q^k, q^{k+1}, ..., is constructed starting from a guessed function q^0. The conjugate gradient technique is used in the determination of the optimization direction. By calculating iteratively

$$q^{k+1} = q^k + \alpha^k p^k \tag{5.7}$$

q finally converges to the optimum position in the function space $L^2[D, [0, t_f]]$.

The conjugate technique is essentially the same as in the steady problem except that the functional space is different. The scalar β^k is now given by

$$\beta^k = \frac{\langle (\nabla E^k - \nabla E^{k-1}), \nabla E^k \rangle_{L^2[D,[0,t_f]]}}{\|\nabla E^{k-1}\|^2_{L^2[D,[0,t_f]]}} \tag{5.8}$$

while the conjugate direction is still

$$p^k = -\nabla E(q^k) + \beta^k p^{k-1}. \tag{5.9}$$

5.2.1 Definition of Gradient and Sensitivity Problem

The gradient of $E(q)$, at point q, denoted by $\nabla E(q)$, for time-dependent problem, is related to the variation of E at this point as in the steady problem. Recall that the directional derivative of E at q in the direction Δq, denoted by $D_{\Delta q}E(q)$, is defined by

$$D_{\Delta q}E(q) = \lim_{\epsilon \to 0} \frac{E(q + \epsilon \Delta q) - E(q)}{\epsilon} \tag{5.10}$$

and it is related to the gradient $\nabla E(q)$ by

$$D_{\Delta q}E(q) = \langle \nabla E(q), \Delta q \rangle_{L^2[D,[0,t_f]]}. \tag{5.11}$$

That is

$$\begin{aligned} D_{\Delta q}E(q) &= \int_0^{t_f} \int_D \nabla E(q(r,t)) \Delta q(r,t)\, dD\, dt \\ &= \int_0^{t_f} \int_0^1 \nabla E(q(y,t)) \Delta q(y,t)\, dy\, dt. \end{aligned} \tag{5.12}$$

As in Chapter IV, the temperature sensitivity $\tilde{T}$ in time-dependent problem is defined as the directional derivative of T at q in the direction Δq, i.e.,

$$\tilde{T}(x,y,t) = D_{\Delta q}T(x,y,t:q). \tag{5.13}$$

Based on the above definitions and Eq. 2.9, the sensitivity problem is readily derived as

$$\nabla^2 \tilde{T} = \frac{\partial \tilde{T}}{\partial t} \tag{5.14}$$

with the conditions

$$\begin{cases} \tilde{q} = \Delta q & at \quad x = 0; \\ \tilde{q}_0 = 0 & at \quad x = L; \\ c_{11}\tilde{T} + c_{12}\dfrac{\partial \tilde{T}}{\partial y} = 0 & at \quad y = 0; \\ c_{21}\tilde{T} + c_{22}\dfrac{\partial \tilde{T}}{\partial y} = 0 & at \quad y = 1; \\ \tilde{T}_0(x,y) = 0 & at \quad t = 0. \end{cases} \tag{5.15}$$

The optimization step α is given by

$$\alpha = -\frac{< \nabla E, p >_{L^2[D,[0,t_f]]}}{\|\tilde{T}\|^2_{L^2[D_m,[0,t_f]]}}. \tag{5.16}$$

5.2.2 The Adjoint Problem

For the time-dependent problem, the adjoint problem is

$$\nabla^2 T^* = -\frac{\partial T^*}{\partial t} \tag{5.17}$$

with the conditions

$$\begin{cases} q^* = 0 & at \quad x = 0; \\ q_0^* = T_m - T & at \quad x = L; \\ c_{11}T^* + c_{12}\dfrac{\partial T^*}{\partial y} = 0 & at \quad y = 0; \\ c_{21}T^* + c_{22}\dfrac{\partial T^*}{\partial y} = 0 & at \quad y = 1; \\ T^*(x,y) = 0 & at \quad t = t_f. \end{cases} \tag{5.18}$$

It appears that the driving force of the adjoint problem is the error between the given temperatture measurements $T_m(y,t)$ and calculated temperature T at $x = L$.

Recall that the gradient $\nabla E(q)$ is related to its directional derivative by

$$D_{\Delta q}E(q) = \int_0^{t_f} \int_D \nabla E(q)\Delta q\, dD\, dt. \tag{5.19}$$

Also it can be derived from Eq. 5.5 that

$$D_{\Delta q}E(q) = \int_0^{t_f} \int_{D_m} (T - T_m)\tilde{T}(D_m, t)\, dD_m\, dt. \tag{5.20}$$

From Eq. 5.19 and Eq. 5.20 we then deduce

$$\int_0^{t_f} \int_D \nabla E(q)\Delta q\, dD\, dt = \int_0^{t_f} \int_D T^*(D,t)\Delta q\, dD\, dt \tag{5.21}$$

which implies that the gradient of the object functional $\nabla E(q)$ is equal to the adjoint temperature at the boundary where the heat flux $q(y,t)$ is applied, i.e.,

$$\nabla E = T^*(D,t) = T^*(0,y,t). \tag{5.22}$$

Note that in solving the adjoint equation, we have imposed an unphysical end condition, namely that the adjoint temperature be zero at the final time. The heat flux remains therefore the same as its first guessed value at the final time, independently of the number of iterations. Errors committed at the final time thus propagate back to early times, i.e., against the parabolic nature of the heat equation.

5.2.3 Numerical Implementation

As for the steady IHCP, the minimization process consists of three direct problems for each iteration. An implicit control volume approach (Patankar [57]) is used to discretize these three equations. The discreted equations are solved by alternating line and column sweeps by the Thomas algorithm at each time step. For the adjoint equation, the algorithm first makes the change of variable

$$\tau = t_f - t \tag{5.23}$$

and starts with the condition at the physical time $t = t_f$ so that, via this transformation, the adjoint problem is an initial value problem in τ.

The optimization algorithm procedure for time-dependent problem can be summarized as follows [24].

1. Choose initial guess $q^0(y,t)$ and set iteration counter $k = 0$;

2. Solve the direct problem with $q^k(y,t)$ to obtain $T^k(x,y,t)$ and calculate the current value of

$$\begin{aligned} E(q^k) &= \frac{1}{2} \parallel T(r,t:q) - T_m(r,t) \parallel^2_{L^2[D_m,[0,t_f]]} \\ &= \frac{1}{2} \int_0^{t_f} \int_0^1 (T^k(L,y,t) - T_m(y,t))^2 \, dy \, dt, \end{aligned} \tag{5.24}$$

If $E(q^k) < \epsilon$ or $k \geq k_{max}$, stop;

3. Evaluate the error $T^k(D_m,t) - T_m(y,t)$ on the boundary D_m;

4. Solve the adjoint problem backward in time to obtain $T^{*k}(x,y,t)$;

5. Evaluate the gradient $\nabla E^k = T^{*k}(0,y,t)$;

6. Calculate the search direction p^k by

$$p^k = \begin{cases} -\nabla E^k, & if \quad k = 0 \\ -\nabla E(q^k) + \beta^k p^{k-1}, & if \quad k > 0 \end{cases} \tag{5.25}$$

where

$$\beta^k = \frac{< \nabla E^k - \nabla E^{k-1}, \nabla E^k >_{L^2[D,[0,t_f]]}}{\|\nabla E^{k-1}\|^2_{L^2[D,[0,t_f]]}}; \tag{5.26}$$

7. Solve the sensitivity problem with $\Delta q = p^k$ on the predicted boundary D to obtain $\tilde{T}^k(x,y,t)$;

8. Calculate the step size by

$$\alpha = -\frac{< \nabla E, p >_{L^2[D,[0,t_f]]}}{\|\tilde{T}(D_m)\|^2_{L^2[D_m,[0,t_f]]}}; \tag{5.27}$$

9. Update

$$q^{k+1} = q^k + \alpha^k p^k; \tag{5.28}$$

10. Set $k = k + 1$, go back to step 2, repeat until convergence criterion is satisfied.

Attention must be given to the choice of a proper initial flux q^0 which is crucial for the convergence of the minimization process. In fact, since the adjoint temperature vanishes at $t = t_f$, the conjugate gradient method will always lead to

$$q^k(r, t_f) = q^0(t_f), \tag{5.29}$$

therefore convergence may be non-uniform and very slow if started with an unrealistic guess.

5.3 Solution Analysis

As an example, we first solve the unsteady heat conduction equation Eq. 5.1 with the conditions

$$\begin{cases} T = T_m(y,t) & at \quad x = L; \\ q_0 = 0 & at \quad x = 1; \\ \dfrac{\partial T}{\partial y} = 0 & at \quad y = 0; \\ \dfrac{\partial T}{\partial y} = 0 & at \quad y = 1; \\ T(x,y) = 0 & at \quad t = 0 \end{cases} \tag{5.30}$$

where T_m is generated from the direct problem

$$\begin{cases} q = \dfrac{\partial T}{\partial x} = cos\pi y \, sin\pi t & at \quad x = 0; \\ q_0 = 0 & at \quad x = 1; \\ \dfrac{\partial T}{\partial y} = 0 & at \quad y = 0; \\ \dfrac{\partial T}{\partial y} = 0 & at \quad y = 1; \\ T(x,y) = 0 & at \quad t = 0. \end{cases} \tag{5.31}$$

The exact inverse solution for q is obviously the one used in the direct problem, i.e., $cos\pi y \, sin\pi t$.

A 21 × 21 mesh is used, and $t_f = 3$. The initial guess is $q^0 = 0$. Exact and optimization result of $q(y,t)$ (after 10 itrs.) as well as $q(0.25,t)$ are shown by Fig. 5.1 and Fig. 5.2. It can be seen that the numerical result matches the exact solution well except near $t = t_f$. This can be overcome by using longer t_f.

As shown from the steady problem from Chapter IV, the truncation errors may

play an important role in the precision of the solution: For higher frequency (along y) boundary heat flux such as $q = cos2\pi y$ and $L = 1$, q always keeps its initial guessed value without moving toward the expected solution, due to truncation errors that make the step size α vanishingly small.

Just as in the steady problem, we may reach the right solution if the sensors and the unkown boundary are closer enough. Fig. 5.3 shows the numerical results for the case with $q = cos2\pi y$ and sensors located at $x = 0.5$. Fig. 5.4 is the exact solution. The optimization result is good except near $t = t_f$.

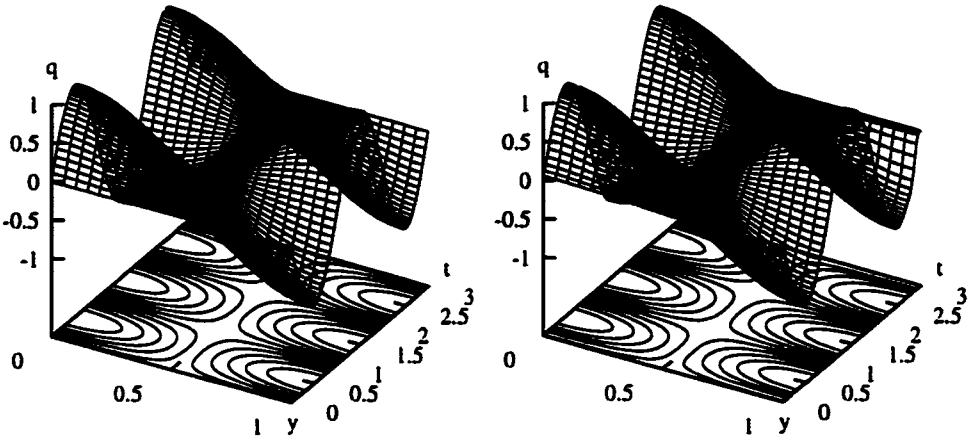

Figure 5.1: Optimization and exact result of $q = cos\pi y\, sin\pi t$, $L = 1$

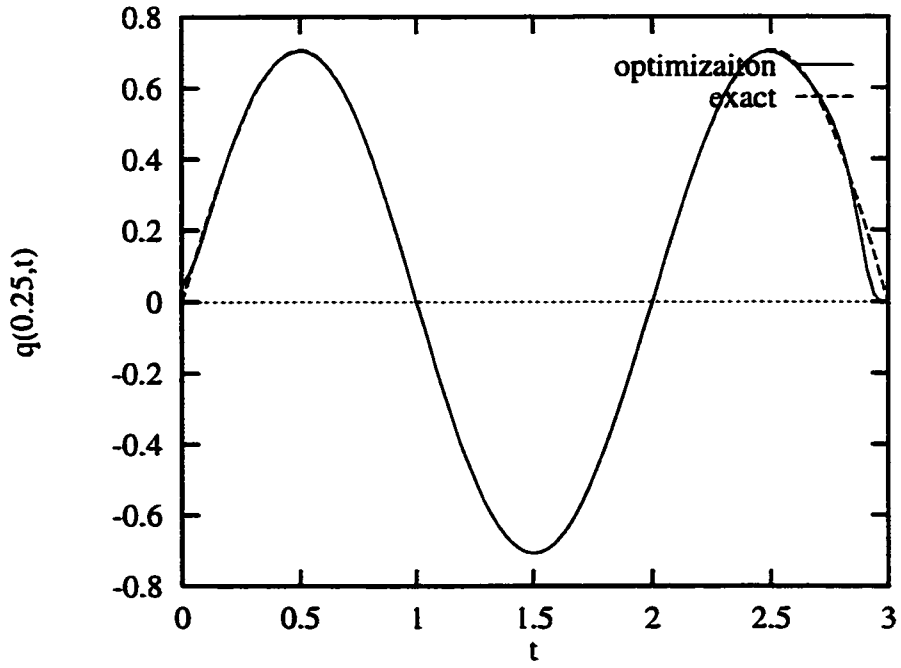

Figure 5.2: Comparison of optimization and exact result of $q(0.25, t)$

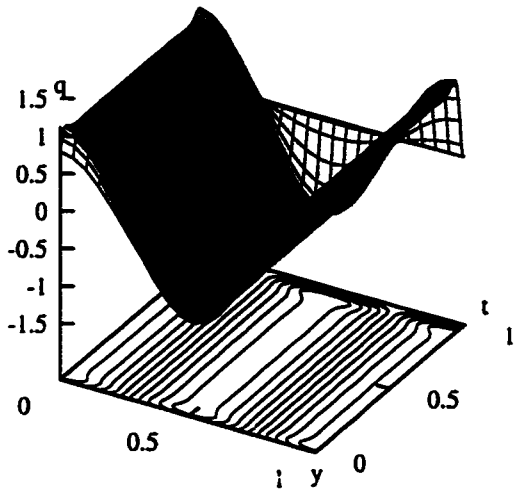

Figure 5.3: Optimization result of $q = cos2\pi y$, $L = 0.5$

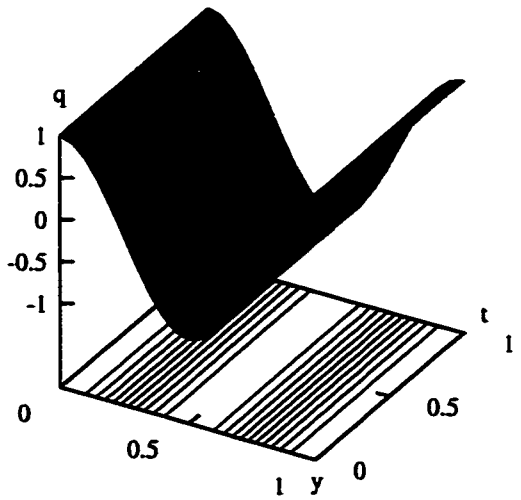

Figure 5.4: Exact result of $q = cos2\pi y$, $L = 0.5$

5.3.1 Spatial Errors

Because it is a time-dependent problem, measurement errors of T_m happen along both position y and time t. It is necessary to study these errors separately as spatial and temporal errors.

The effect of the spatial random noise on the solution may be analyzed by firstly considering single-frequency signals. Cases with the following conditions are tested.

$$\begin{cases} T = T_m(y) & at \quad x = L; \\ \dfrac{\partial T}{\partial x} = 0 & at \quad x = L; \\ \dfrac{\partial T}{\partial y} = 0 & at \quad y = 0; \\ \dfrac{\partial T}{\partial y} = 0 & at \quad y = 1; \\ T_0(x, y) = 0 & at \quad t = 0 \end{cases} \tag{5.32}$$

where T_m is chosen respectively to be $0.01\,sin\pi y$, $0.01\,sin4\pi y$, $0.01\,sin10\pi y$ or $0.02\,rand$, with $rand$ being a random number between -0.5 and 0.5.

Fig. 5.5 - Fig. 5.8 are the results of $q(y, t)$ obtained after 20 iterations. To show the difference of making measurements at different distances from the unknown boundary, T_m is applied at $x = 1$ and $x = 0.5$.

These results agree with those of steady problem. From these figures one can also see that:

1) Except for some initial and final time steps, the results with T_m at $x = 0.5$ obviously have oscillations while the results with T_m at $x = 1$ are almost flat around 0. That is to say that when the distance is relatively far, T_m has small effect in q;

2) The magnitude of the error in q depends on the distance of the two boundaries.

The closer the two boundaries are, the smaller the magnitude is.

5.3.2 Temporal Errors

Temporal errors are studied the same way as spatial error, some cases as Eq. 5.32 are tested with $T_m = 0.01\,sin\pi t$, $0.01\,sin5\pi t$, $0.01\,sin10\pi t$ and $0.02\,rand(t)$ at $x = 1$ and $x = 0.5$. The recovered heat flux is shown in Fig. 5.9 - Fig. 5.12.

Fig. 5.9 - Fig. 5.12 show that temporal errors do not behave in the same way as spatial errors. Note that because the results of $q(y,t)$ do not vary along y, they are presented as the function of only t.

From these figures we may note that

1) Higher frequency components in the given data yield higher value for the predicted heat flux;

2) By moving the sensors closer to the unknown boundary, the recoverd heat flux is smaller, i.e., higher-frequency errors in the given data will have smaller effects on the predicted heat flux.

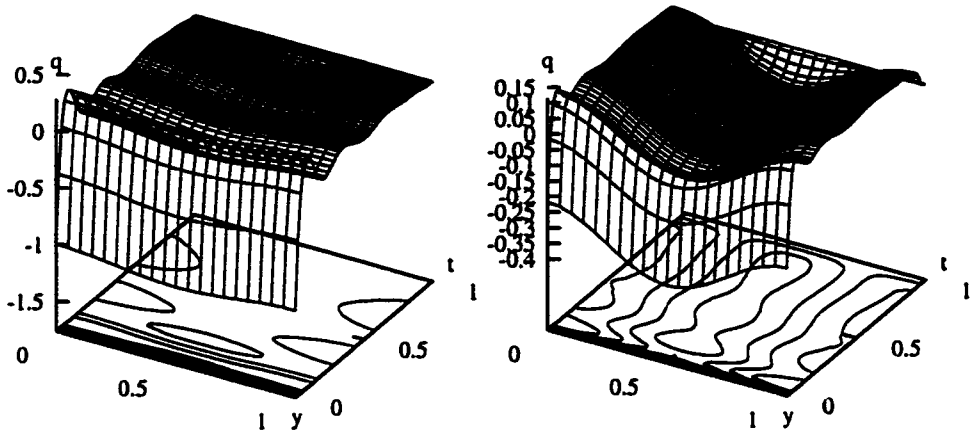

Figure 5.5: $T_m = 0.01\, sin\pi y$ at $x = 1$ and $x = 0.5$

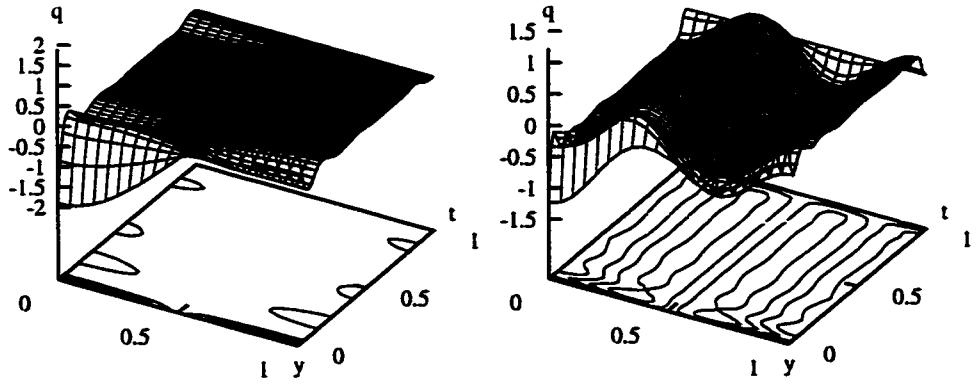

Figure 5.6: $T_m = 0.01\, sin4\pi y$ at $x = 1$ and $x = 0.5$

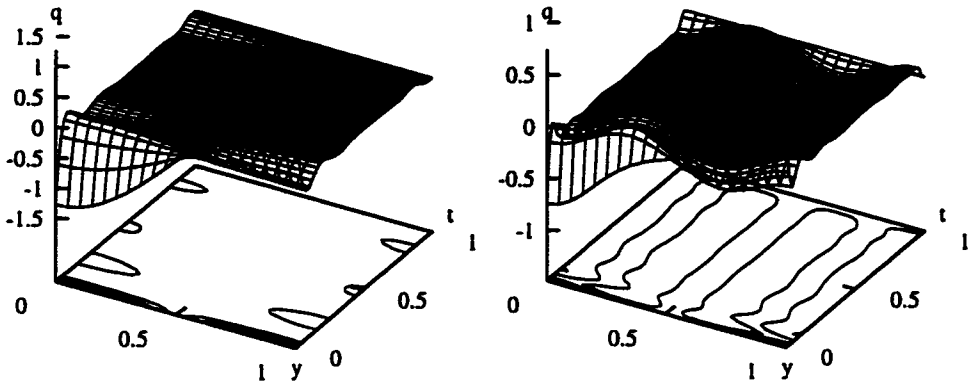

Figure 5.7: $T_m = 0.01 \, sin 10\pi y$ at $x = 1$ and $x = 0.5$

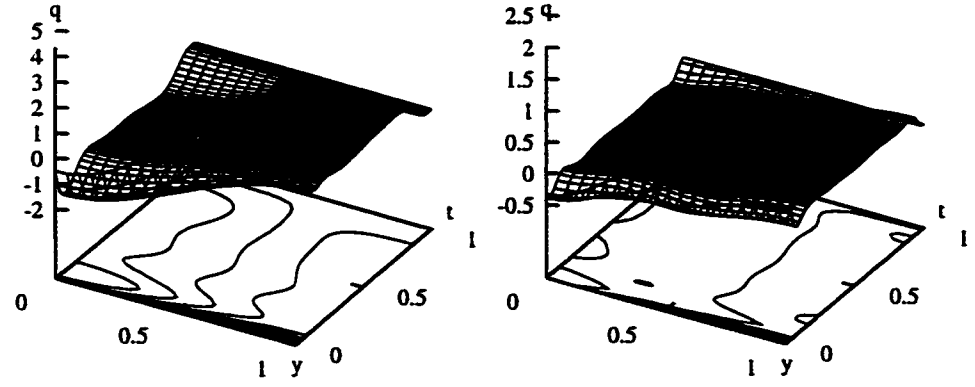

Figure 5.8: $T_m = 0.02 \, rand(y)$ at $x = 1$ and $x = 0.5$

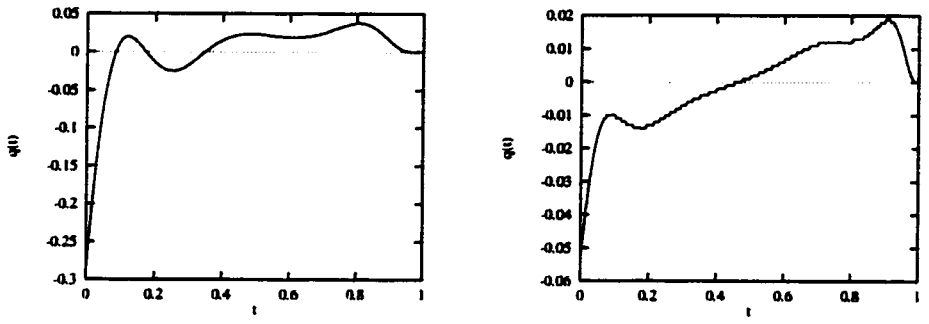

Figure 5.9: $T_m = 0.01\, sin\pi t$ at $x = 1$ and $x = 0.5$

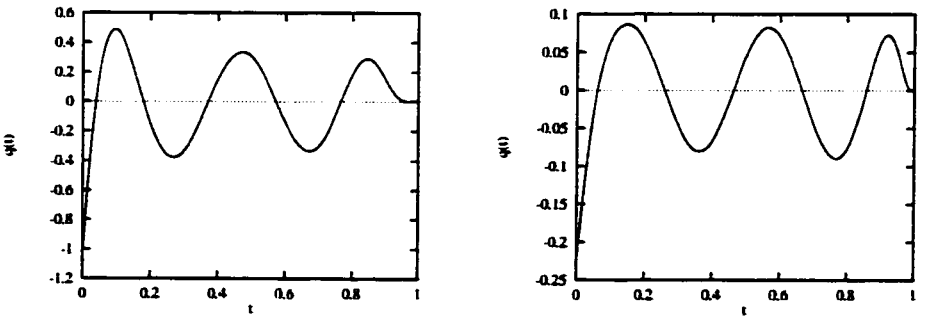

Figure 5.10: $T_m = 0.01\, sin5\pi t$ at $x = 1$ and $x = 0.5$

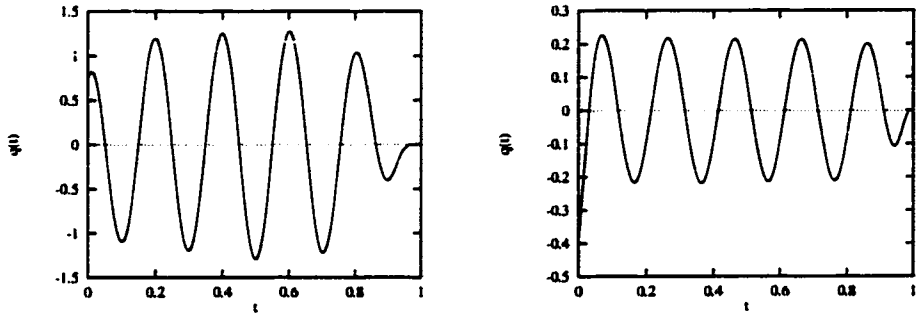

Figure 5.11: $T_m = 0.01\, sin 10\pi t$ at $x = 1$ and $x = 0.5$

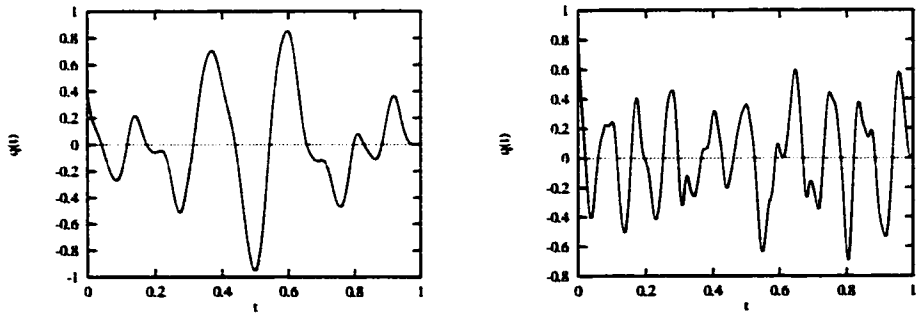

Figure 5.12: $T_m = 0.02\, rand(t)$ at $x = 1$ and $x = 0.5$

5.3.3 Regularized Solutions

The mollification method was studied in Chapter III. It turned out to have limited use in the marching method mainly because the mollification might also eliminate useful information besides the noise, especially when applied at every step of maching process. Here in the optimization method, it is worthy of trying to apply only once a filter to T_m in order to reduce the magnitude of the noise on T_m and thus the result error at predicted q.

The Gaussian filter is adopted to smooth the random error $T_m = 0.02\,rand(y)$ and $T_m = 0.02\,rand(t)$ of last cases. From Fig. 5.13 and Fig. 5.14 one can see that their error magnitudes are greatly reduced as expected, compared to Fig. 5.8 and Fig. 5.12.

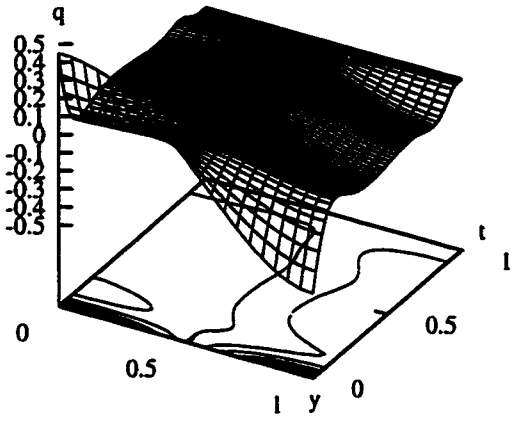

Figure 5.13: $T_m = 0.02\,rand(y)$ (smoothed by Gaussian filter) at $x = 1$

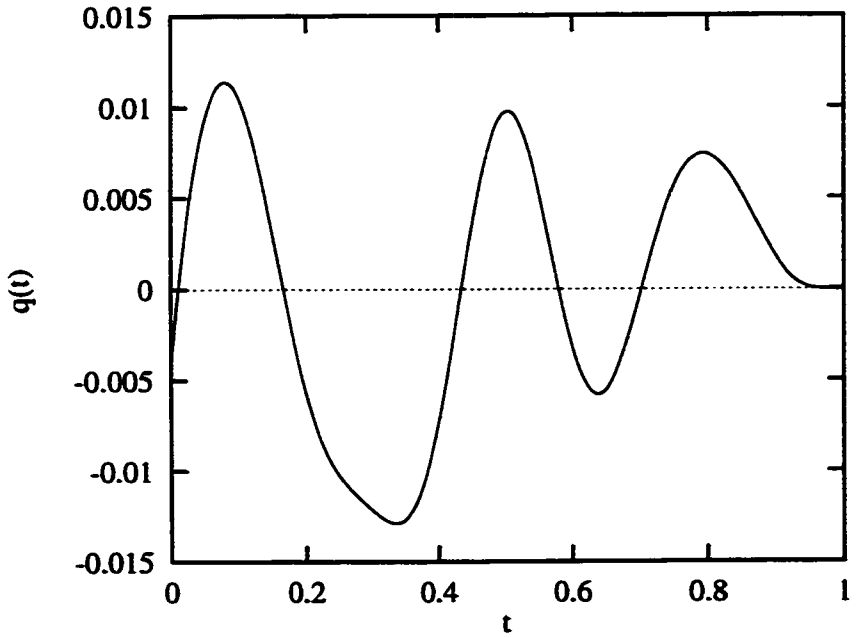

Figure 5.14: $T_m = 0.02\,rand(t)$ (smoothed by Gaussian filter) at $x = 1$

CHAPTER VI

CONCLUSION

The objective of this thesis is to solve the ill-posed 2D IHCP by two different methods, namely the space marching method and the optimization method by conjugate gradient. The work thus consists essentially of two parts: The first part is devoted to the method of solving the 2D IHCP by space marching in conjunction with the mollification technique. The second part is devoted to the optimization method by conjugate gradient.

In each case, the effects of numerical errors and measurements errors on the inverse solutions are anlyzed at each step of the algorithm. The regularization effects of filtering by mollification and iteration are next analyzed in details.

The results of this study may be summarized as follows.

Following an introduction to the general IHCP in Chapter 1, the description and formulation of the 2D IHCP are given in Chapter 2. The main results are presented in Chapter 3, 4 and 5.

In Chapter 3, it is shown that the space marching method is very unstable not

only against random errors in the given data, but also against numerical errors which are generated by computational truncations at each and every step of the marching process. In other words, if the marching process is started with exact given data and performed with absolute accuracy, we then arrived at an exact solution for the boundary heat flux. However, if either the given data are inexact, or the marching process is executed with some computational errors, the solution will unconditionally blow up due to the exponential growth of these errors as we march toward the unknown boundary. It was shown that the development of these instabilities depends strongly on the relative grid size as well as on the cavity size. In retrospect, it is quite reasonable to expect that the marching method is unconditionally unstable, as it directly solves the 2D IHCP in the original form of an initial-value problem with Cauchy data. In order to suppress these instabilities, it seems quite natural to suppress their origin, i.e., both the experimental and computational errors! This can be done by applying a low-pass filter at every step of the marching process. Although filtering technique is efficient to suppress high-frequency noises, it may also distort the "true" temperature field. We thus observed a strong effect of filtering at the end points, due to extrapolation beyond the given domain. The errors committed at these end points actually propagate into interior points, especially if the filter is applied repeatly during the marching process. The distorsion of the solution, as well as the suppression of undesired high-frequency noises, depend sensibly on the type of filter and the number of times it is applied. Among the three types of filters considered, namely the Square filter, the Dirichlet filter and the Gaussian filter, it was found that the last one may be a good choice for a good number of unknown functions.

Chapter 4 considers the 2D IHCP from an optimization point of view. The problem then consists of finding iteratively a boundary heat flux that would induce a temperature as close as possible to the one measured by sensors located within

the given cavity. This amounts to solving a minimization problem in an infinite-dimensional function space by the conjugate gradient technique. The corresponding iterative algorithm was analyzed by comparing the analytical and numerical results obtained for the case of steady 2D IHCP with given data decomposed in Fourier series. It was found that numerical truncation errors also strongly affect the final results, but in a very different way from the space-marching method: Here, due to the diffusive nature of the heat equation, high-frequency components of the boundary heat flux die off much faster than low-frequency components. As they become vanishingly small, they "get lost" in the round-off errors of the numerical computations in various steps of the algorithm. More specificly, it was found that numerical errors make the step size in the search direction vanishingly small compared to the analytical value as the frequency of the given data is increased and/or the sensors are moved further away from the unknown boundary. Therefore, convergence towards the expected value can not be reached. From a practical point of view, this may be considered as a beneficial regularization effect in the sense that if the high-frequency components of the data one due to measurement errors, they will not affect the solutions! However, if these high-frequency components are parts of the real data, then the corresponding boundary heat flux that causes them can not be recovered! By looking for a "right" position to place the sensors, we may therefore arrive at an solution with acceptable accuracy and stability.

We next analyzed the convergence mechanism of the iterative conjugate gradient algorithm by considering given data with multifrequency components. It was found that as the iteration progresses, the first iteration recovers mainly the lowest frequency component of the unknown heat flux, the second iteration yields the next higher frequency component, and so on. Very high frequency components will be recovered only at high iteration number. This is the very desirable regularization effect intrinsically embedded in the iterative algorithm of solution by conjugate gra-

dient. In other words, a choice can be made of an optimum iteration number to arrive at a regularized solution with acceptable accuracy and stability.

Finally, the time-dependent 2D IHCP was considered within the optimization approach by conjugate gradient and mollification techniques. It was verified that the results found in the two previous chapters for the steady state 2D IHCP also apply to the time-dependent 2D IHCP: Using the conjugate gradient technique in conjunction with a low-pass Gaussian filter applied only once to the given data (polluted with random noises), a very smooth and accurate solution was obtained by an appropriate combination of sensors' positions and iteration number.

Based on the results obtained in this study, we may make the following recommendation for solving the ill-posed 2D IHCP:

1. For on-line (real time) diagnostic and control purposes where a rough estimate of boundary heat flux is acceptable and a fast prediction is necessary, space marching technique may be used with an appropriate choice of a low-pass filter.

2. For an accurate prediction of boundary heat flux or for more general inverse heat transfer problems, the conjugate gradient method should be used in conjunction with a low-pass filter applied to the given data.

BIBLIOGRAPHY

[1] O. M. ALIFANOV. *Inverse Heat Transfer Problems.* Springer-Verlag, New York, 1994.

[2] O. M. ALIFANOV, E. A. ARTYUKHIN, and S. V. RUMYANTSEV. *Extreme Methods for Solving Ill-Posed Problems with Applications to Inverse Heat Transfer Problems.* Begell House, New York, 1996.

[3] O. M. ALIFANOV and N. V. KEROV. Determination of external thermal load parameters by solving the two-dimensional inverse heat conduction problem. *Journal of Engineering Physics*, 41(4):1049–1053, 1981.

[4] C. H. HUANG and M. N. OZISIK. Direct integration approach for simultaneously estimating temperature dependent thermal conductivity and heat capacity. *Numerical Heat Transfer, Part A*, 20:95–110, 1991.

[5] C. KRAVARIS and J. H. SEINFELD. Identification of parameters in distributed parameter systems by regularization. *SIAM J. Contr. Optimization*, 23:217–241, 1985.

[6] C. E. MEJIA and D. A. MURIO. Numerical identification of diffusivity coefficient and initial condition by discrete mollification. *Computers Math. Applic.*, 30:35–50, 12 1995.

[7] N. ZABARAS, Y. RUAN, and O. RICHMOND. On the design of two-dimensional Stefan processes with desired freezing front motions. *Numer. Heat Transfer*, 21B:307–325, 1992.

[8] N. ZABARAS. Inverse finite element techniques for the analysis of solidification processes. *Int. j. numer. methods engr.*, 29:1569–1587, 1990.

[9] N. ZABARAS and S. KANG. On the solution of an ill-posed inverse design solidification problem using minimization techniques in finite and infinite dimensional spaces. *Int. j. numer. methods engr.*, 36:3973–3990, 1994.

[10] S. KANG and N. ZABARAS. Control of the freezing interface motion in two-dimensional solidification processes using the adjoint method. *Int. j. numer. methods engr.*, 38:63–80, 1995.

[11] N. ZABARAS and T. Hung NGUYEN. Control of the freezing interface morphology in solidification processes in the presence of natural convection. *Int. j. numer. methods engr.*, 38:1555–1578, 1995.

[12] J. R. CANNON and C. D. HILL. Existence, uniqueness, stability, and monotone dendence in a Stefan problem for the heat equation. *J. Math. Mech.*, 17:1–19, 1967.

[13] D. L. COLTON and R. REEMTSEN. The numerical solution of the inverse Stefan problem in two space variables. *SIAM J. Appl. Math.*, 44:996–1013, 1984.

[14] J. HADAMARD. Sur les problèm aux derivees partielles et leur signification physique. *Bull. Univ. Princeton*, 13:49–52, 1952.

[15] Dinh Nho HAO. *Inverse Heat Conduction Problems, Dr. rer. nat. Dissertation.* PhD thesis, Mathematics Department, Freie Universitat Berlin (West), 1991. 199 pages.

[16] J. HADAMARD. Lectures on Cauchy's problem in linear partial differential equations. Technical report, Dover, New York, 1952.

[17] A. MOUTSOGLOU. An inverse convection problem. *Heat Transfer ASME*, 111:37–43, 1989.

[18] O. M. ALIFANOV and Yu. V. EGOROV. Algorithms and results of solving the inverse heat conduction problem in a two-dimensional formulation. *Journal of Engineering Physics*, 48(4):489–496, 1985.

[19] E. A. ARTYUKHIN and I. Yu. GEDZHADZE. Sequential regularization solution of a boundary inverse heat conduction problem. 2nd Joint Russian-America Workshop on Inverse Problems in Engineering, St. Petersberg, Russia, August 1994.

[20] T. HSU, N. SUN, G. CHEN, and Z. GONG. Finite element formulation for two-dimensional inverse heat conduction analysis. *ASME Journal Heat Transfer*, 114:553–557, 1992.

[21] H. J. REINHARDT and N. H. HAO. A sequential conjugate gradient method for the stable numerical solution to inverse heat conduction problems. *Inverse Problems*, 2:263–272, 1996.

[22] H. J. REINHARDT and N. H. HAO. On the numerical solution of inverse heat conduction problems by gradient methods. In K. Woodbury D. Delaunay and M. Raynaud, editors, *Proceeding of the Second International Conference on Inverse Problems in Engineering: Theory and Pracdce*, LeCroisic, France, June 1996. ASME Engineering Foundation.

[23] Z. R. LI, M. PRUD'HOMME, and T. H. NGUYEN. A numerical solution for the inverse natural convection problem. *Numer. Heat Transfer, Part B*, vol. 28:307–321, 1995.

[24] T. H. NGUYEN. Optimization approach to the inverse convection problem. In *Proc. Intl. Workshop Inv. Prob.*, pages 83–90, Ho-Chi Minh City, Vietnam, 1995.

[25] T. H. NGUYEN. An optimization approach to some inverse convection problems. In *Proc. Intl. Conf. Analysis and Mechanics of Continuous Media*, pages 188–195, Ho-Chi Minh City, Vietnam, 1995.

[26] T. H. NGUYEN. Inverse convection problems : A preview. In *Proc. 2nd Intl Thermal Energy Congress*, pages 1–11, Agadir, 1995.

[27] M. PRUD'HOMME and T. H. NGUYEN. A whole time-domain approach to the inverse natural convection problem. *Num. Heat Transfer, Part A*, 1997. in press.

[28] A. M. OSMAN and J. V. BECK. Investigation of transient heat transfer coefficients in quenching experiments. *ASME Journal Heat Transfer*, 112:843–848, 1990.

[29] O. R. BURGGRAF. An exact solution of the inverse problem in heat conduction theory and applications. *ASME J. Heat Transfer*, 86C:373–382, 1964.

[30] J. V. BECK, B. BLACKWELL, and C. R. JR. ST. CLAIR. *Inverse Heat Conduction, Ill-posed Problems.* Wiley-Interscience, New York, 1985.

[31] D. A. MURIO. *The Mollification Method and the Numerical Solution of Ill-posed Problem.* John Wiley, New York, 1993.

[32] E. HENSEL. *Inverse Theory and Applications for Engineers.* Prentice Hall, Englewood Cliffs, N. Y., 1991.

[33] J. V. BECK, B. BLACKWELL, and R. S. JR. ST. CLAIR. Efficient sequential solution of the nonlinear inverse heat conduction problem. *Numer. Heat Transfer*, 5:275–286, 1982.

[34] J. V. BECK and D. A. MURIO. Combined function specification-regularization procedure for solution of heat conduction problems. *AIAA J.*, 24:180–185, 1986.

[35] B. F. BLACKWELL. Efficient technique for the numerical solution of the one-dimensional inverse problem of heat conduction. *Numer. Heat Transfer*, 4:229–238, 1981.

[36] B. J. BLACKWELL. Some comments on Beck's solution of the inverse problem of heat conduction through the use of Duhamel's theorem. *Inter. J. Heat Mass Transfer*, 26:302–305, 1983.

[37] R. G. HILLS and E. C. Jr. HENSEL. One-dimensional nonlinear inverse heat conduction technique. *Numer. Heat Transfer*, 10:369–393, 1986.

[38] R. G. HILLS and G. P. MULHOLLAND. The accuracy and resolving power of one dimensional transient inverse heat conduction theory as applied to discrete and inaccurate measurements. *Int. J. Heat Mass Transfer*, 22:1221–1229, 1979.

[39] R. G. HILLS, M. RAYNAUD, and E. HENSEL. Surface variance estimates using an adjoint formulation for one-dimensional nonlinear inverse heat conduction technique. *Numer. Heat Transfer*, 10:441–461, 1986.

[40] L. GUO and D. MURIO. A mollified space marching finite difference algorithm for the two-dimensional inverse heat conduction problem with slab symmetry. *Inverse Problems*, 7:247–259, 1991.

[41] L. GUO, D. A. MURIO, and C. ROTH. A mollified space marching finite difference algorithm for the inverse heat conduction problem with slab symmetry. *Comput. Math. Appl.*, 19:75–89, 1990.

[42] A. CARASSO. Space marching difference schemes in the nonlinear inverse heat conduction problem. *Inverse Problems*, 8:25–43, 1992.

[43] A. N. TIKHONOV. *Solutions of Ill-Posed Problems.* Halsted Press, Washington; Winston; New York, 1977.

[44] P. NEITTAANMAKI and D. TIBA. *Optimal Control of Nonlinear Parabolic Problems.* Marcel Dekker, Inc., New York, 1994.

[45] J. BAUMEISTER. *Stable Solution of Inverse Problems.* Vieweg & Sohn, Braunschweig/Wiesbaden, 1987.

[46] J. V. BECK. Nonlinear estimation applied to the nonlinear inverse heat conduction problem. *Inter. J. Heat Mass Transfer*, 13:703–716, 1970.

[47] J. V. BECK. Criteria for comparison of methods of solution of the inverse heat conduction problem. *Nucl. Eng. Des.*, 53:11–22, 1979.

[48] Dinh Nho HAO. A non-characteristic Cauchy problem for linear parabolic equations and related inverse problems I: Solvability. *Inverse Problems*, 10:295–315, 1994.

[49] Dinh Nho HAO. A non-characteristic Cauchy problem for linear parabolic equations and related inverse problems II: Avariational method. *Pitman Res. Notes in Maths*, 263:43–56, 1992.

[50] Dinh Nho HAO. Regularization of a noncharacteristic Cauchy problem for the heat equation. *Math. Meth. in the Appl. Sci.*, 15:537–545, 1992.

[51] Dinh Nho HAO. A mollification method for ill-posed problems. *Numer. Math.*, 68:469–506, 1994.

[52] Dinh Nho HAO and H. J. REINHARDT. Stable numerical solution to linear inverse heat conduction problems by the conjugate gradient methods. *J. Inverse and Ill-Posed Problems*, 3:447–467, 1995.

[53] Dinh Nho HAO and H. J. REINHARDT. Recent contributions to linear inverse heat conduction problems. *J. Inverse and Ill-Posed Problems*, 4:23–32, 1996.

[54] A. M. OSMAN, K. J. DOWDING, and J. V. BECK. Numerical solution of the general two-dimensional inverse heat conduction problem (IHCP). *ASME Jounal of Heat Transfer*, 119:38–45, 1997.

[55] Patrick J. ROACHE. *Elliptic Marching Methods and Domain Decomposition.* CRC Press, Inc., 1995.

[56] C. E. MEJIA and D. A. MURIO. Numerical solution of generalized IHCPby discrete mollification. *Computers Math. Applic.*, 32:33–50, 2 1996.

[57] Suhas V. PATANKAR. *Numerical Heat Transfer and Fluid Flow.* Hemisphere Publishing Corporation, 1980.

[58] P. CRAVEN and G. WAHBA. Smoothing noisy data with spline functions. *Numer. Math.*, 31:377–403, 1979.

[59] P. K. LAMN. Future-sequential regularization methods for ill-posed Volterra equations: Applications to the inverse heat conduction problem. *J. Math. Analysis and Applications*, 195:469–494, 1995.

[60] Y. JARNY, M. N. OZISIK, and J. P. BARDON. A general optimization method using adjoint equation for solving multidimensional inverse heat conduction. *Int. J. Heat Mass Transfer*, 34:2911–2919, 1991.

[61] R. FLETCHER. *Practical Methods of Optimization.* Wiley-Interscience, New York, 1987.

[62] E. POLAK. *Computational Methods in Optimization.* Academic Press, New York, 1971.